CCR7 Expression Distinguishes Functionally Distinct pTfh1 Subsets with Roles in Malaria-Specific Immunity

Megan SF Soon [1], Damian A Oyong[1], Nicholas Dooley[1] , Reena Mukhiya[1,2,3], Zuleima Pava[1], Dean Andrew[2], Jessica R Loughland[1], James McCarthy[4], Jo-Anne Chan[1,4,5], James G Beeson[1,4,5], Christian Engwerda[2,3], Ashraful Haque[4], Michelle J Boyle[1,3,4,5 #]

1. Burnet Institute, 85 Commercial Road, Melbourne, VIC, Australia
2. QIMR-Berghofer, 300 Herston Road, Herston, QLD, Australia
3. Environment and Sciences, Griffith University, QLD, Australia
4. University of Melbourne, VIC, Australia
5. Monash University

corresponding author: michelle.boyle@burnet.edu.au

Abstract

T-follicular CD4 T (Tfh) cells play essential roles in antibody induction during infection and following vaccination. In humans, peripheral Tfh (pTfh) cells are commonly analysed based on expression of CXCR3 and CCR6, with different subsets of pTfh (pTfh1, pTfh2, pTfh17) associated with antibody induction in a context-dependent manner. In malaria, the specific roles of pTfh subsets in antibody development is not clear. Several studies in human malaria infection and vaccination have identified an important role of pTfh2 cells, which associate with antibody development while pTfh1 cells do not. However, *in vitro* studies and animal models highlight that pTfh1 cells are key drivers of cytophilic antibody development, which are protective. To dissect these contradictions, we mapped the heterogeneity of pTfh cells in healthy donors and individuals with controlled human malaria infection using scRNAseq. We identified two previously unidentified pTfh1-like subsets with functional relevance, which can be defined based on CCR7 expression. CCR7^{pos} pTfh1 cells have increased capacity to produce IL-21, whereas CCR7^{neg} pTfh1 cells express markers of cytotoxicity. In controlled human malaria infection, we show that both CCR7^{pos} and CCR7^{neg} pTfh1 cells, along with Tfh2 cells, clonally expand, are transcriptionally and phenotypically activated, and are malaria specific. However, only CCR7^{pos} pTfh1 and pTfh2 cells associated with antibody responses to infection. Our data expand our knowledge of Tfh cell diversity and function during human infection and resolve contradictions of the role of pTfh1 cells in antibody development targeting malaria. Data advance our knowledge of Tfh cell diversity and may inform approaches to target these key CD4 T cells during vaccination.

Introduction

T-follicular helper (Tfh) cells are the key CD4 T cell subset that function within the germinal centre to support B cell development. Cytokine and receptor mediated signals from Tfh cells, drive B cell selection, support antibody class switching, and differentiation into antibody-producing long-lived plasma cells and memory B cells. Due to the key role of antibodies and memory B cells in protection from most pathogens, Tfh cells are attractive targets to boost naturally acquired or vaccine-mediated protection *(1)*. To develop such therapies, an improved understanding of how Tfh cells drive antibody development in specific disease contexts is required.

While Tfh cells function within the secondary lymphoid tissues such as draining lymph nodes, spleens and tonsils, some Tfh cells, or a subset thereof, also circulate. This allows analysis of peripheral blood to provide a 'snapshot' of the germinal centre response during human infection *(2–5)*. Both GC- and peripheral Tfh cells, identified by expression of C-X-C chemokine receptor 5 (CXCR5) and programmed cell death protein (PD1), can be further analysed as Tfh-subsets, with cells taking on characteristics of CD4+ T cell helper cell lineages *(6)*. The most common strategy to identify pTfh cell subsets is analysis of CXCR3 and CCR6, classifying cells as pTfh1 (CXCR3+/CCR6-), pTfh2 (CXCR3-/CCR6-) and pTfh17 (CXCR3-/CCR6+). Expression of CXCR3 and CCR6 has also been reported on germinal centre (GC) Tfh cells from secondary lymphoid tissues *(3)*. Specific pTfh cell subsets have differing abilities to activate naïve or memory B cells and have been associated with antibody development in a pathogen and vaccine-dependent manner. For example, pTfh2 cells are more able to activate naïve B cells and have been associated with the development of broadly neutralizing antibodies in HIV infection *(7)*. On the other hand, pTfh1 cells robustly activate memory B cells, and are consistently associated with antibodies induced by influenza vaccination *(8, 9)*. Differing functional capacities of pTfh2 cells may be underpinned by 'skewing' of Tfh cells by the cytokine milieu induced during infection or vaccination, allowing Tfh cells to adopt specific roles to influence B cell development *(6)*.

For some infections, the link between specific cytokine-skewed pTfh subsets and antibody development is less clear. In malaria, caused by *Plasmodium* parasites, we have shown that the activation of pTfh2 cells was associated with antibody development during controlled human malaria infection (CHMI) with *P. falciparum* of naïve adults *(10)*. Similarly, pTfh2 cells also associated with induction of antibodies by approved and experimental malaria vaccines *(11–13)*. This association was observed despite the overall response during malaria being dominated by pTfh1 cell activation *(10, 14, 15)*. In Malian children, the robust pTfh1 cell activation was not associated with antibody development following malaria treatment *(15)*. However, recent studies by our team have shown that these relationships are more nuanced, with Ugandan children who had the highest levels of protective antibodies having increased frequencies of activated and proliferating pTfh2, together with pTfh1

70 cells *(16)*. Additionally, parasite activated pTfh1 cells induced T-bet+ B cells with high IgG3
71 expression *(17)*, and IgG3 antibodies are consistently associated with protection from malaria *(18)*.
72 Mouse models of malaria have not clarified these contradictions, with Tfh1 cells being shown to be
73 protective and supporting affinity maturation of B cells in some studies *(19)*, and being suppressers of
74 antibody development in others *(20)*. These contradictory results may be in part due to the limited
75 approaches to identify subsets of pTfh cells. While transcriptional and phenotypic diversity of Tfh
76 have begun to be explored in other infections in mouse models *(21, 22)*, and in small human vaccine
77 studies with influenza and SARS-CoV-2 *(23, 24)*, our understanding of Tfh diversity in malaria
78 infection is currently limited.

79 We hypothesised that there is greater diversity of pTfh cells with distinct functional activities that is
80 currently not understood, in part due to analysis of pTfh in human infection with limited chemokine
81 markers. To address this, we analysed pTfh cells in healthy individuals and during human malaria by
82 applying single cell RNA sequencing (scRNAseq) and multidimensional spectral flow cytometry. We
83 applied these approaches to cell samples from well-defined CHMI cohorts and identified
84 characteristics of antigen specific pTfh subsets associated with antibody development. Our data
85 highlight the phenotypic and functional diversity of Tfh cells during human infection, and nuanced
86 associations with antibody development.

87

88 **Results**

89 **Analysis of pTfh cells with scRNAseq identifies two Tfh1-like subsets**

90 To explore pTfh cell transcriptional heterogeneity and generate a reference map for pTfh cells during
91 human infection, we first performed scRNAseq on pTfh cells sorted from healthy human donors (n=4,
92 sex 50% males, aged 28.5 [25.5-35], median [IQR] years). We sorted three pTfh subsets (pTfh1,
93 pTfh2 and pTfh17 from CXCR5+ PD1+ cells), based on classical definitions of CXCR3/CCR6
94 expression, alongside the less functional or less activated CXCR5+ PD1- compartment (**Fig. 1A,**
95 **Supplementary Fig. S1A**). After QC, a total of 7,302 cells were analysed with high quality cells
96 captured from each donor and subset (pTfh1 n= 2,089, pTfh2 n=717, pTfh17 n=744, PD1- n=2,839,
97 **Supplementary Fig. 1B**). Following data integration by donor (**Supplementary Fig. 1C)**, we
98 identified 11 pTfh cell clusters using a combination of unsupervised and semi-supervised clustering
99 methods (**Fig. 1B-D, Supplementary Table 1**). Two Tfh1 like clusters were identified, both with
100 relatively high expression of *CXCR3* and *CST7* (annotated Tfh1_cytotoxic and Tfh1_CCR7). A Tfh2
101 cluster was identified with high expression of genes associated with GC Tfh cells, including *TOX2*
102 *(25, 26), MAF (27, 28),* and *TCF7*. The signature of this cluster mapped to the majority of tonsil GC
103 Tfh cells in a publicly available data set *(29)* (**Supplementary Fig. 1D**), confirming the

104 transcriptional relationship between Tfh2 cluster and GC Tfh cells identified here and reported
105 previously *(7)*. Tfh17 cluster was annotated based on high expression of genes associated with Th17
106 cells *CCR6, BHLHE40,* and *TGFB1 (30–32)*. Most cells within these Tfh1/Tfh2 and Tfh17
107 transcriptional clusters were sorted from the PD1+ cells (**Fig. 1B/C**). Other transcriptional clusters
108 included cells enriched in Type I IFN genes (annotated as IFNI), a cluster enriched with heat shock
109 proteins (annotated stress), another cluster enriched with ribosomal genes (annotated ribosomal), and
110 two clusters without clear marker genes (cluster 2, possibly a quiescence cell subset, with
111 upregulation of genes *BTG1* and *ZFP36L2,* and cluster 3 which only had limited upregulated genes
112 including annexin family members *ANXA1*, *ANXA2*, *S100A10)* (**Fig. 1D**). Analysis of key T helper
113 genes also identified a small cluster of cells positioned close to the Tfh1 cluster that expressed a
114 mixture of Tfh1/Tfh17 signature, which were manually clustered and annotated as Tfh1.17 (**Fig.**
115 **1B/D**). Additionally, another subset of cells expressing *FOXP3* and Treg signature genes including
116 *CTLA4* was identified manually and annotated as Tfr (**Fig. 1D**). The remaining Tfh cell subsets
117 expressed diverse levels of markers associated with various aspects of Tfh or CD4 T cell
118 development, with no clear patterns of expression across subsets (**Supplementary Fig. 1E**).

119 Comparing the two cell clusters identified as pTfh1 cells, the Tfh1_cytotoxic cluster had high
120 expression of *GZMK*, *GZMM*, *CCL5* and *NKG7* (**Fig. 1D/E, Supplementary Fig. 1E,**
121 **Supplementary Table 2)**. The signature of the Tfh1_cytotoxic annotated cells overlaps with
122 cytotoxic Tfh cells previously identified in mice models, including the increased expression of
123 *EOMES (33)*, and in a recent small analysis of human Tfh cells from the periphery and tonsil
124 *(34)* (**Supplementary Fig. 1E)**. Potentially cytotoxic, granzyme-K expressing pTfh cells have also
125 recently been identified in type-1 skewed response in mice, and in human CMV specific pTfh cells
126 *(21)*. In contrast, the Tfh1_CCR7 cluster had lower expression of cytotoxic markers, and instead had
127 increased expression of *CCR7* and *SELL.* Differential expression of CCR7 along with PD1 has
128 previously been used to differentiate Tfh subsets within CXCR5+ cells in both mice and humans, with
129 $CCR7^{lo}/PD1^{hi}$ described as effector cells and $CCR7^{hi}/PD1^{lo}$ described as resting cells *(35)*. However
130 here, both Tfh1_cytotoxic and Tfh1_CCR7 subsets largely existed in clusters that were from the
131 PD1+ sorted populations thus identifying an unappreciated gradient of CCR7 expression within PD1+
132 cells (**Fig. 1C/F, Supplementary Fig. 1F).** Pathway analysis of Tfh1_CCR7 and Tfh1_cytotoxic
133 cluster marker genes highlighted the shared and divergent transcriptional signatures of these cells
134 (**Supplementary Fig. 1G**). For example, both subsets were enriched for 'Th1 pathway', and
135 'Interferon gamma signalling', while only Tfh1_CCR7 cells were enriched in 'Th2 pathway' and
136 'ICOS-ICOSL Signalling in T Helper Cells' suggesting potential functional differences between the
137 two transcriptional clusters (**Supplementary Fig. 1G**).

138 To dissect the relationship between Tfh cell transcriptional and phenotypic characteristics, the degree
139 of overlap between designated Tfh cell subsets and sorted cell phenotypes was analysed.

140 Tfh1_cytotoxic, Tfh1_CCR7, Tfh2 and Tfh17 clusters, defined by transcriptional profiles, were
141 mainly found in cells expressing *PDCD1*. Further, *CXCR3* and *CCR6* expression overlapped with the
142 pTfh1 and Tfh17 sorted populations, respectively, suggesting some overlap between transcriptional
143 clusters and those identified via CXCR3 and CCR6 expression (**Fig. 1C**). However, *CCR4* expression,
144 often used to define Th2 cells, overlapped in both pTfh2 and pTfh17 sorted clusters and had the
145 highest expression in Tfh17 and Tfr transcriptional clusters (**Supplementary Fig. 1E**). Nearly all cells
146 found within both Tfh1 transcriptional clusters (Tfh1_cytotoxic and Tfh1_CCR7), were from the
147 pTfh1 sorted cell population. However, the sorted pTfh1 population also contained cells from all other
148 transcriptional subsets. Similarly, the phenotypic pTfh2 population was dominated by the Tfh2
149 transcriptional subset, but also contained cells with diverse transcriptional annotations (**Fig. 1F,**
150 **Supplementary Fig. 1F**). This pattern was also seen for the phenotypic pTfh17 population. The PD1-
151 phenotypic cells contained cells of all clusters, but were dominated by IFNI, stress, ribosomal and
152 cluster 2 and cluster 3 cells.

153 To understand the clonal sharing between clusters, TCR sequences were analysed. TCR sequences
154 with complete TRA/TRB genes were captured for 3,998 (55.6%) cells. Clones were defined by the
155 sharing of identical amino acid sequences. While the majority of TRA/TRB cells were singletons
156 (3839 clones), clonal expansion was detected in 159 cells across 57 clones ranging in size from 2 to
157 20 identical clones. Clonal expansion was detected particularly within the Tfh1_cytotoxic subset
158 (**Supplementary Fig. 1H**). As expected, no clones were shared across individuals (**Supplementary**
159 **Fig. 1I**) Within each clonotype, we examined the fate sharing clones to investigate if clones of the
160 same family tend to share the same transcriptional subsets or were found across diverse Tfh
161 phenotypes. 40/57 clonotypes (70.2%) were found in a single subset. Clonal sharing was evident
162 between Tfh1_cytotoxic and Tfh1_CCR7 but not Tfh2 transcriptional clusters, while Tfh2 shared
163 clones with ribosomal, cluster 2 and cluster 3 cells (**Fig. 1G**). Together, these data show that while
164 commonly used phenotypic markers CXCR3 and CCR6 can resolve some heterogeneity in pTfh cells,
165 additional diversity, particularly within pTfh1 cells is identified when analysing underlying
166 transcriptional profiles of pTfh cells. Transcriptional profiles suggest that this diversity has potential
167 functional relevance in antibody development.

168

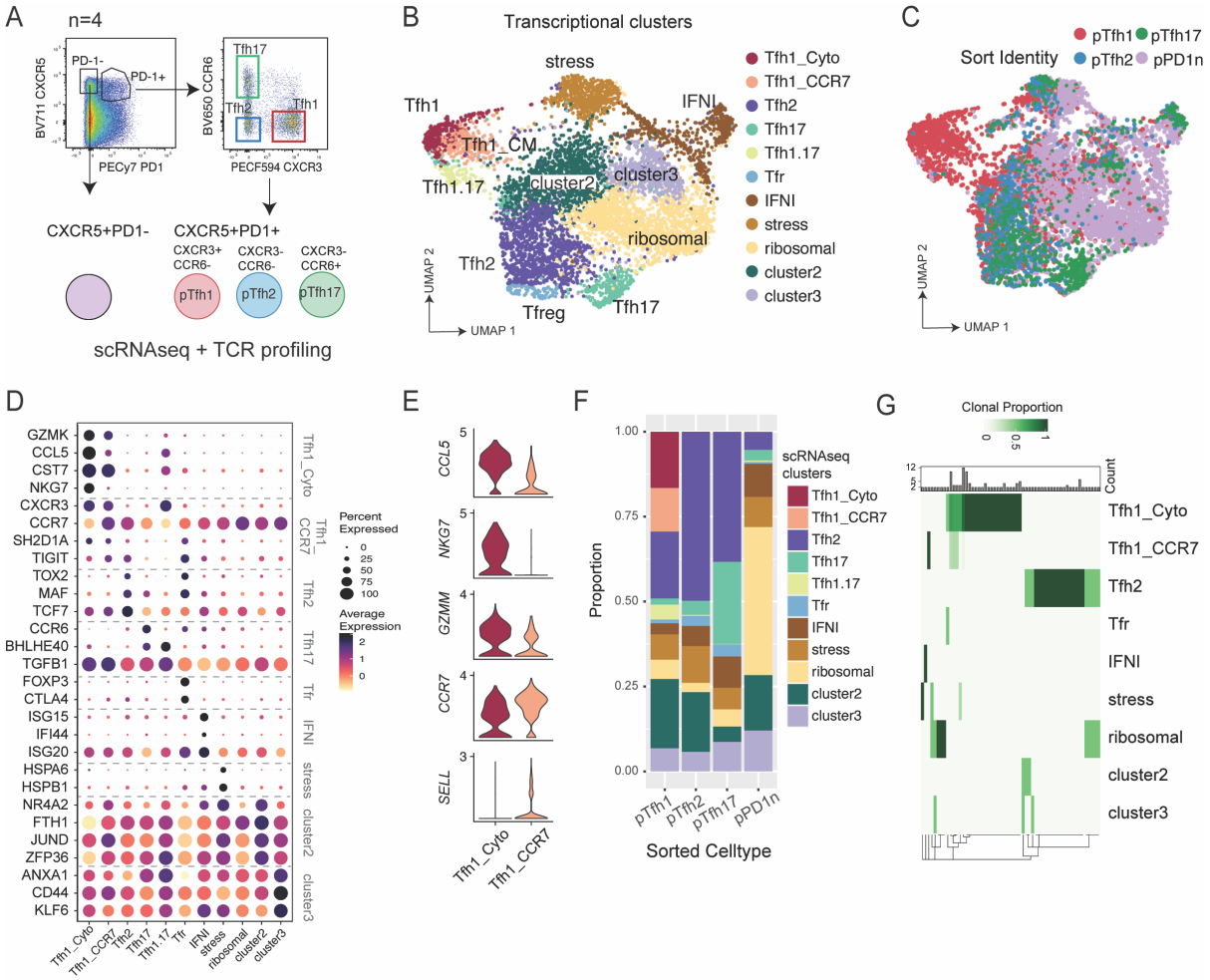

Fig. 1. scRNAseq analysis of pTfh cells from healthy individuals
__A.__ Four populations were sorted from pTfh CD4+ cells from 4 healthy donors - 1) CXCR5+PD1-, 2) CXCR5+PD1+ pTfh1, 3) CXCR5+PD1+ pTfh2, and 4) CXCR5+PD1+ pTfh17. Populations were analysed by 5' droplet scRNAseq for gene expression and TCR sequence. __B.__ UMAP of data following integration by donor, with 11 transcriptional subsets indicated. __C.__ UMAP of data depicting cell sorted identity. __D.__ Relative gene expression of genes used to annotate transcriptional clusters. __E.__ Selection of key genes differentially expressed between Tfh1_Cyto and Tfh1_CCR7 annotated transcriptional clusters. __F.__ Relationship between cell sorted identity and transcriptional cluster identity in the data set. __G.__ Fate sharing at the individual clonotype level across transcriptional subsets. Expanded clonotypes ($n^3 2$) with only same fates (exist within the same subset), or different fates are shown See also Supplementary Fig. 1 and Supplementary Table S1 and S2.

pTfh1 subsets have distinct phenotypic characteristics and functional potential

Transcriptional analysis identified two pTfh1-like subsets with distinct expression of cytotoxic and memory associated genes. To explore these pTfh1 subsets at the protein level, along with pTfh2 and pTfh17 cells, we designed a comprehensive phenotyping panel for pTfh cells which included commonly assessed chemokine receptors (CXCR3 and CCR6), markers identified in our transcriptional data set or previously used *(36)* (including CCR7, and cytotoxic markers) and transcriptional factors with reported roles in Tfh cell function or development (**Supplementary Table**

190 **S3)**. pTfh cell subsets were analysed within healthy human donors (n= 19, sex 83.3% males, aged 24
191 years [20.2-28.2, median [IQR] years). Within pTfh cells (CXCR5+PD1+ CD4 T cells) a gradient of
192 CCR7 expression was detected, including within pTfh1 cells (**Fig. 2A, Supplementary Fig. 2A**).
193 Within pTfh subsets, expression of cytotoxic markers NKG7, GrzmB and GrzmK was significantly
194 higher in CCR7^{neg} pTfh1 compared to either CCR7^{pos} pTfh1 or pTfh2 and pTfh17 cells, consistent
195 with scRNAseq analysis and suggesting that cytotoxic potential of pTfh cells is restricted to pTfh1
196 CCR7^{neg} subsets (**Fig. 2B-D, Supplementary Fig. 2B**). Transcriptional analysis also suggested that
197 Tfr cells were more closely related to pTfh2 subsets. This was also confirmed phenotypically where
198 there was a relatively increased proportion of FoxP3+CD25+ pTfh cells within the pTfh2 cell subset
199 **(Supplementary Fig. 2C**).

200 Within pTfh cells, we also quantified expression of cMaf which was upregulated in Tfh2 cell clusters
201 and SAP (*SH2D1A)* which was a marker of Tfh1_CCR7 (**Fig. 1D**), both of which have essential roles
202 in GC Tfh cell development *(37)*. cMaf expression was not different between pTfh1 CCR7$^{neg/pos}$ cells,
203 both of which had significantly lower expression compared pTfh2 and pTfh17, consistent with
204 previous reports *(7)* (**Fig. 2E, Supplementary Fig. 2B**). SAP expression was low across all subsets,
205 and was lowest in pTfh2, and comparable between the two pTfh1 subsets (**Fig. 2F**). We also assessed
206 TIGIT which is reported to have highest expression in GC-Tfh and pTfh2 cells *(7)*, and which was
207 relatively higher in Tfh1_CCR7 cells compared to Tfh1_cytotoxic cells transcriptionally (**Fig. 1D**). In
208 contrast to our transcriptional data and previous reports, TIGIT expression was highest on pTfh1
209 CCR7^{neg} cells compared to both pTfh1 CCR7^{pos} and pTfh2 cells (**Fig. 2G**). The function of TIGIT+
210 pTfh cells is unclear, with both reports of TIGIT+ pTfh having both enhanced *(38)* and reduced
211 capacity *(39)* to provide B cell help and associated with antibody development help depending on the
212 disease context. Thus, different findings on TIGIT expression on pTfh cell subsets may be
213 underpinned by the experimental models analysed.

214 To assess pTfh cell subset diversity with an unbiased approach, all pTfh cells were analysed with
215 unsupervised clustering based on expression of CXCR3, CCR6, CCR7, NKG7, GrzmB, GrzmK,
216 cMAF, TIGIT and FoxP3. Unbiased clustering consistently identified two subsets of pTfh1 cells
217 based on CCR7 expression, where CCR7^{neg} cells also expressed high levels of NKG7, GrzmB and
218 GrzmK (**Fig. 2H, Supplementary Fig. 2D-F).** pTfh2, pTfh17 and pTfh1-17 cells could also be
219 identified (**Fig. 2H**). Additionally, FoxP3+ Tfr cells were identified and clustered within the pTfh2
220 cell subset, consistent with scRNAseq data, and reflected in manual gating (**Supplementary Fig. 2C**).

221

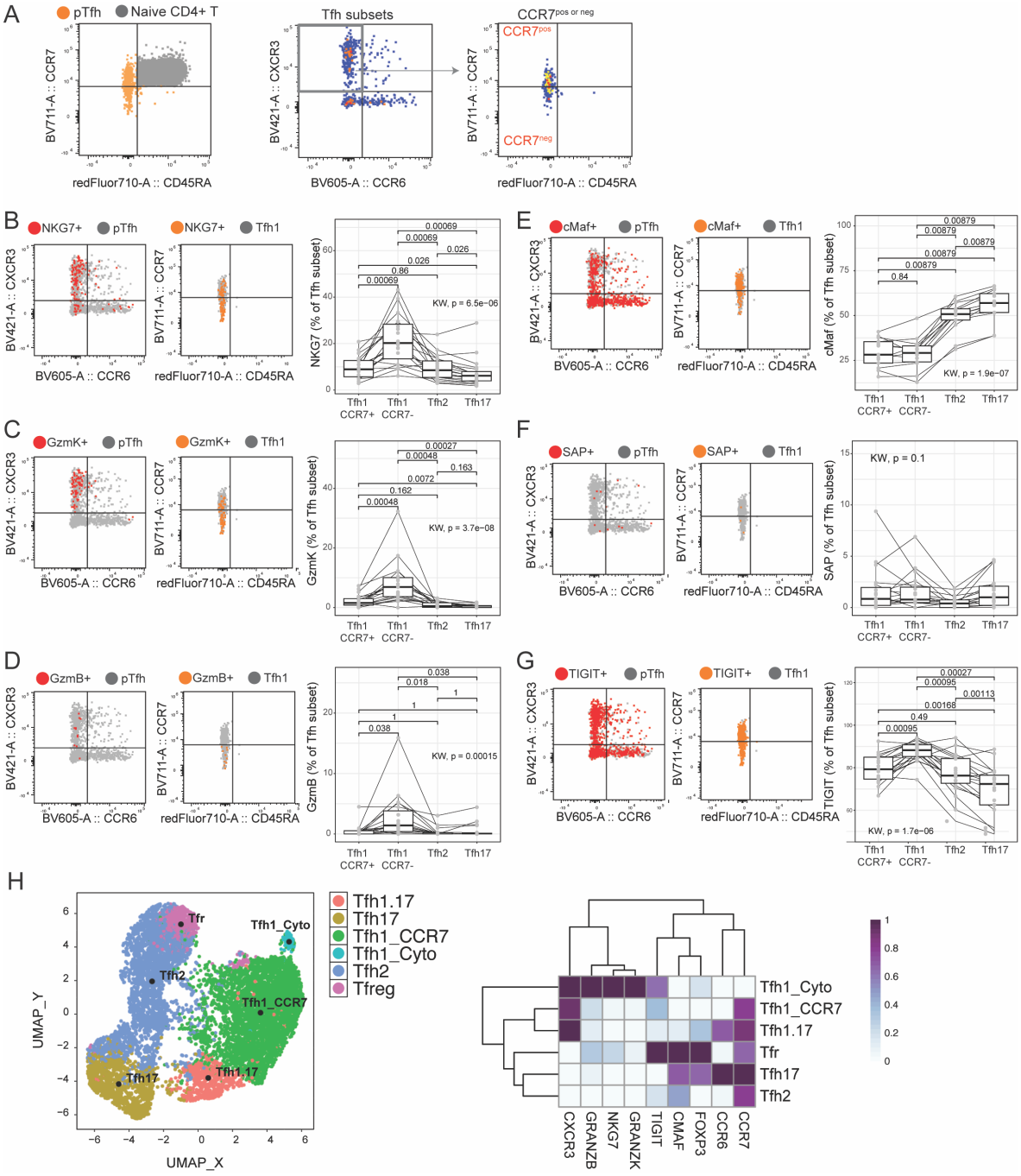

Figure 2: Phenotypic diversity of pTfh cell subsets based on CCR7 expression.
A comprehensive spectral flow cytometry panel was used to analyse pTfh cells in healthy individuals (n =19). ***A)*** *A gradient of CCR7 expression is detected within pTfh cells, and pTfh1 CCR7neg (CCR7-) and pTfh1 CCR7pos (CCR7+) subsets can be identified, along with pTfh2 and pTfh17 cells.* ***B-D)*** *Expression of cytotoxic markers NKG7, Granzyme K and Granzyme B (**B**) and cMaf, SAP **(C)**, and TIGIT **(D)** were analysed within pTfh cell subsets. Flow plots are a representative individual with marker expression overlayed against CXCR3 and CCR6 or CCR7 and CD45RA. Boxplots with median and IQR are indicated along with individuals. P is the paired Wilcoxon signed-rank test after adjustment with multiple testing correction using Holm's method, while the Kruskal-Wallis test is used for the global comparison.* ***(E)*** *pTfh cells were analysed with unbiased analysis of indicated markers. UMAP of a single experiment analysing n=7 individuals. Analysis performed three independent times. See also Supplementary Fig. 2.*

236 To further investigate functional relevance of pTfh1 cell subsets, cytokine production from pTfh cells
237 was quantified following PMA/Io stimulation in healthy donors (**Supplementary Fig. 3,**
238 **Supplementary Table S4,** n=11, sex 36.36 % males, age 37.5[32-40], median[IQR] years). As seen
239 *ex vivo*, a gradient of CCR7 expression is detected within pTfh1 cell subsets identified with CXCR3
240 and CCR6 expression post stimulation (**Fig. 3A**). Following PMA/Io stimulation and within the
241 commonly identified pTfh1, pTfh2 and pTfh17 cell subsets, the production of the Tfh-related cytokine
242 IL-21 was comparable, while pTfh1 produced higher IFNγ and TNF, pTfh2 produced higher IL-4 and
243 pTfh17 produced higher IL-17, as expected (**Fig. 3B**). Production of the regulatory cytokine IL-10
244 was detected at low levels in all subsets. When pTfh1 cells were analysed based on CCR7 expression,
245 pTfh1 CCR7^{pos} cells produced significantly higher levels of IL-21, relative to pTfh1 CCR7^{neg} cells
246 (**Fig. 3C**). Further, when the total cytokine composition was analysed, there was a significant
247 difference in the cytokine composition produced by pTfh1 CCR7^{pos} compared to CCR7^{neg} cells (**Fig.**
248 **3D).**

249 Together, these data show that transcriptionally, phenotypically and functionally, pTfh1 cell subsets
250 identified by CXCR3+ expression can be further distinguished based on CCR7 expression. pTfh1
251 CCR7^{pos} cells having higher functional potential, while the expression of markers associated with
252 cytotoxic potential are restricted to pTfh1 CCR7^{neg} cells. These data highlight a previously
253 unrecognised diversity of pTfh cells in healthy individuals when only considering subsets identified
254 by CXCR3 and CCR6 expression, which may have important implication to B cell development
255 during infection.

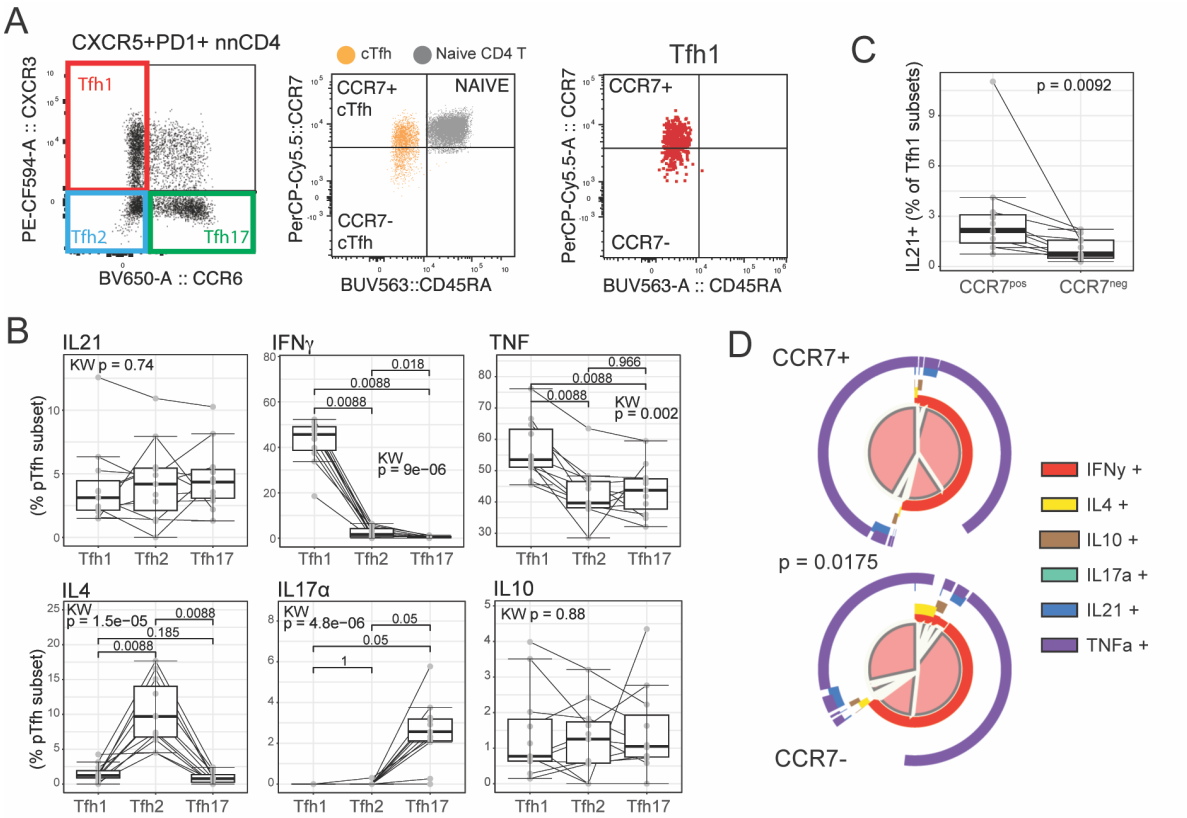

Figure 3. Functional diversity within pTfh cell subsets based on CCR7 expression

Cytokine production following PMA/ Io stimulation was measured by intracellular staining in healthy individuals (n=11). ***A)*** *pTfh cells subsets were identified by CXCR3 and CCR6 expression as pTfh1 (CXCR3+CCR6+), pTfh2 (CXCR3-CCR6-) and pTfh17 (CXCR3-CCR6+), and pTfh1 cells identified as CCR7^{pos} and CCR7^{neg} cells.* ***B)****. IL-21, IFNγ, TNF, IL-4, IL-17, and IL-10 expression within pTfh cell subsets. P is the paired Wilcoxon signed-rank test after adjustment with multiple testing correction using Holm's method, while the Kruskal-Wallis test is used for the global comparison.* ***C).*** *IL-21 cytokine expression in pTfh1 cell subsets based on CCR7 expression. P is paired Wilcoxon signed-rank test.* ***D)****Overall cytokine production within pTfh1 CCR7^{pos} and CCR7^{neg} cells. P is permutation test in SPICE. Box and whisker plots indicate first and third quartiles for hinges, median line and lowest and highest values no further than 1.5 IQR from hinges. All individual data are represented by the grey dots and lines. See also Supplementary Fig. 3.*

Expansion of pTfh1 cell subsets in human malaria infection

To investigate the roles of pTfh1 CCR7^{pos} and pTfh1 CCR7^{neg} subsets, along with other pTfh cells, during infection, we applied findings to human malaria with samples from a CHMI study cohort. pTfh cells (CD45RA-CXCR5+PD1+) were sorted from individuals in CHMI at day 0 (prior to inoculation), day 8 (peak infection), day 15 and day 36 (both after anti-parasitic drug treatment), and their transcriptional profiles analysed using 5' droplet scRNAseq (n =4, 100 % males, age 22 [21.5-26], median [IQR] years, **Supplementary Fig. 4A/B**). After QC, 27,552 cells were analysed, with high quality cells captured from each donor and timepoint (day 0 n = 6,741, day 8 n=6,125, day 16 n=8,103, day 36 n=7,583, **Supplementary Fig. 4C**). Data were integrated based on donor and time

281 point **(Supplementary Fig. 4D),** and pTfh cell clusters identified by label transfer with scType (an
282 automated cell-type identification tool *(40)*), using the top 20 upregulated and downregulated marker
283 genes for each cell cluster identified in the healthy 'map' data set used as a reference
284 (**Supplementary Table S5**, **Supplementary Fig. 4E-H**). scType specificity scores were used to
285 collapse clusters into cell subsets (**Figure 4A, Supplementary Fig. 4H**). This approach identified
286 Tfh1_cytotoxic, Th1_CCR7, Tfh2, Tfh17, IFNI, stress, ribosomal, cluster 2 and cluster 3 subsets.
287 Tfh1.17 and Tfr cells were not included in the reference map because of overlapping signatures with
288 Tfh1/Tfh17 and Tfh2 subsets. Following label transfer, Tfh1.17 could not be identified manually,
289 however Tfr cells were identified by inspection of marker genes *FOXP3, CTLA4* and *IL2RA* (**Fig.
290 4B**). Gene expression of annotated cell clusters was consistent with the reference data set (**Fig. 4B,
291 Supplementary Fig. 4G, Supplementary Table S6**). For example, Tfh1_cytotoxic and Tfh1_CCR7
292 clusters both expressed *CXCR3*, with the two clusters having differing levels of inflammatory markers
293 including *GZMK*, *CCL5* and *NKG7,* which were increased in Tfh1_cytotoxic, and the memory
294 markers *SELL* and *CCR7,* which were increased in Tfh1_CCR7 (**Fig. 4B)**. Similarly, Tfh17 cells
295 identified with label transfer had increased expression of *CCR6*, *BHLHE40* and *TNFRSF4*.
296 Interestingly, *TCF7*, *MAF* and *TOX2*, which were identified as marker genes in the reference data set
297 for Tfh2, were expressed both within the Tfh2 subset, but also relatively increased in the Tfh1_CCR7
298 cells in the infection data set (**Fig. 4B, Supplementary Fig. 4G).** Together, these data show the utility
299 of the reference map data set to identify Tfh cell subsets within sorted pTfh cells during multiple time
300 points in infection.

301 To investigate how the Tfh cell compartment was impacted by malaria, we assessed the proportion of
302 each cluster over time. There was a clear expansion of the Tfh1_CCR7 subset in all individuals at day
303 16 post infection, while Tfh1_cytotoxic cells were expanded at this time point to a lesser magnitude
304 (**Fig. 4C**). Tfh2 cells expanded in three of four individuals at day 8, consistent with the earlier
305 activation of this subset in this cohort reported previously *(10)*. Other subsets were not clearly
306 impacted by infection (**Supplementary Fig. 4I)**. Within each subset, TCRA/B sequences were
307 analysed. TCR sequences with complete TRA/TRB genes were captured for 21,939 (77.97%) cells,
308 and this was comparable across the days/cell types (**Supplementary Fig. 5A**). Clones were defined as
309 cells sharing identical amino acid sequence in both TRA and TRB. During CHMI there was evidence
310 of clonal expansion at day 16, with a significant increase in clonal family size greater than 1 (**Fig.
311 4D/E**), and increased Simpson Index, indicating increased clonal expansion (**Fig. 4F**). Expansion was
312 highest in Tfh1_cytotoxic and Tfh1_CCR7 clusters, consistent with the increased frequency of these
313 cells and indicative of clonal proliferation (**Fig. 4E, Supplementary Fig. 5B**). Clonal expansion was
314 also detected within Tfh2 cells at day 16 (**Fig. 4E**). As expected, minimal clonal sharing was detected
315 between donors with only a single clone shared between donor 0 and donor 1 on day 36, which may
316 indicate sequence convergence detected due to analysis of clones with amino acid rather than

317 nucleotide sequence *(41, 42)* (**Supplementary Fig. 5C**). All other clonal sharing occurred within an
318 individual, the majority at a single timepoint (**Supplementary Fig. 5D**). For donor 3, clones were also
319 shared across time points including day 0 prior to malaria, with large clonal families maintaining a
320 single fate across time in the Tfh1_cytotoxic cell cluster, possibly indicating a subset expansion
321 during a prior infection (**Supplementary Fig. 5D**). At day 16, where malaria associated expansion
322 was most evident, clonal sharing across Tfh cell clusters were analysed. While there was a minimal
323 sharing between Tfh1_cytotoxic and Tfh2 cell subsets, Tfh1_CCR7 cells shared clones with both
324 Tfh1_cytotoxic and Tfh2 cells, consistent with the overlapping profiles of Tfh1_CCR7 with both
325 Tfh1_cytotoxic and Tfh2 subsets (**Fig. 4G**). Taken together, these data are consistent with the
326 emergence of malaria specific Tfh cells with diverse transcriptional signatures during infection. These
327 include pTfh1 CCR7^{pos} cells with increased functional capacity, pTfh1 CCR7^{neg} cells with cytotoxic
328 phenotypes, and pTfh2 cells which are transcriptionally most similar to GC Tfh cells *(7)*.

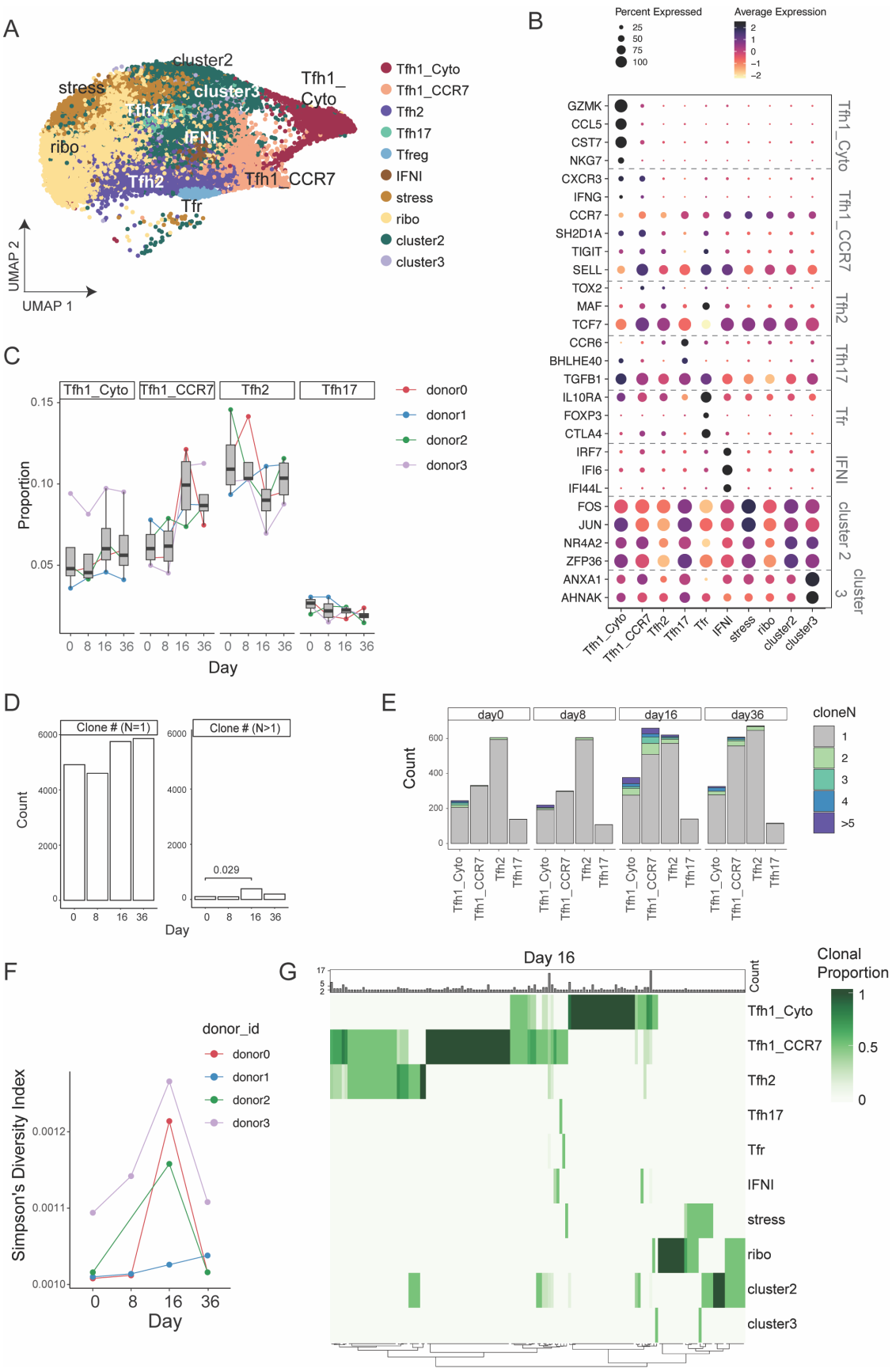

329

330 ***Figure 4: Clonal expansion of diverse pTfh cell subsets during malaria infection***

331 ***A)*** *pTfh cells (CXCR5+PD1+nnCD4 T cells) were isolated from individuals (n=4) during controlled*
332 *human malaria infection (CHMI) at day 0, 8, 16 and 36. scType label transfer was used to identify Tfh*
333 *transcriptional subsets using the healthy Tfh cell data set as a reference.* ***B.*** *Relative expression of*
334 *marker genes used to annotate reference data set in each subset in CHMI data set* ***C.*** *Relative*
335 *proportion of each pTfh transcriptional cluster during CHMI. Each individual is show. Statistical*
336 *testing was not performed due to limited sample size in scRNAseq data set.* ***D.*** *Counts of clones with*
337 *either a clone size = 1 (top) or clone size ≥ 2 across days (bottom). Clonal expansion was detected at*
338 *day 16.* ***E.*** *Clone family size count over time in each subset - Clonal expansion was detected in*
339 *Tfh1_cyto, Tfh1_CCR7 and Tfh2 clusters at day 16.* ***F.*** *Simpsons diversity Index in each donor across*
340 *time.* ***G.*** *Clonal overlap at day 16 across clusters. Clonal size is indicated in count in top bar, each*
341 *clonal proportion across subsets is indicated. See also Supplementary Fig. 4 and 5.*
342
343
344

345 **Unique transcriptional activation of Tfh1 subsets during human malaria infection**

346 To investigate transcriptional pathways activated in each Tfh transcriptional subset during malaria,
347 differential gene expression between day 0 and subsequent time points was performed with pseudo-
348 bulk analysis, grouped by individual (**Supplementary Table S7**). The largest transcriptional changes
349 were detected at day 16 within the Tfh1_CCR7 and Tfh1_cytotoxic subsets (**Fig. 5A**). Differentially
350 expressed genes (DEGs) at day 16 were also detected in Tfh2 cells consistent with clonal expansion
351 of these cells, and previously reported findings *(10)* (**Fig. 5A**). The number of DEGs was contracted
352 by day 36, with DEGs detected at this time point restricted to Tfh1_CCR7, suggesting this subset had
353 a sustained response to infection. The majority of DEGs at day 16 from Tfh1_CCR7, Tfh1_cytotoxic,
354 and Tfh2 were subset specific (**Fig. 5B**). Shared across all three subsets was the activation marker
355 *CD38*, and Tfh1_cytotoxic and Tfh1_CCR7 cells also both upregulated *MKI67* consistent with
356 proliferation and clonal expansion of these cells during malaria. However, overall expression of
357 activation and proliferation genes was highest in Tfh1_CCR7 cells (**Fig. 5C, Supplementary Fig.**
358 **6A**). Analysis of the top 20 upregulated genes from Tfh1_CCR7, Tfh1_cytotoxic and Tfh2 cells
359 highlighted the uniquely upregulated gene signatures identified from Tfh1_CCR7 and Tfh1_cytotoxic
360 cells (**Fig. 5D, Supplementary Fig. 6D**). Additionally, while shared upregulated genes also included
361 genes associated with increased inflammation and cytotoxicity including *NKG7, CCL5, GZMH,*
362 *CXCR3* and *IFNG* the level of these genes was significantly higher in Tfh1_cytotoxic cells (**Fig. 5D**,
363 **Supplementary Fig. 6B**). Further, the transcriptional profile of Tfh2 cells was also maintained and
364 similar to that seen at day 0, despite upregulation of Tfh1 associated genes (**Supplementary Fig. 6C**).
365 Taken together, scRNAseq analysis of pTfh cells during malaria identify the activation, proliferation
366 and clonal expansion of Tfh1_CCR7, Tfh1_cytotoxic and Tfh2 cells with unique transcriptional
367 activation profiles.

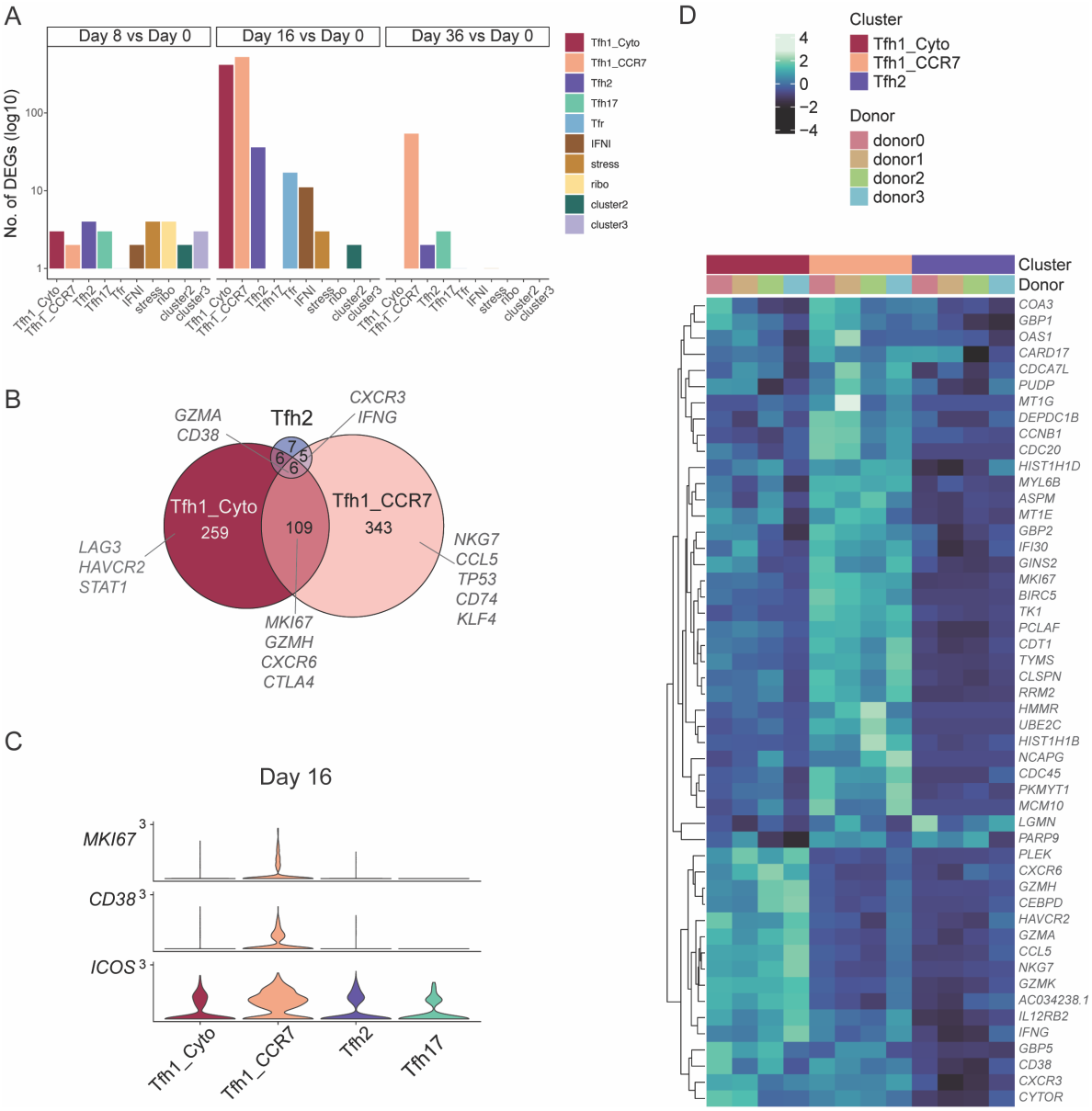

Figure 5: Transcriptional activation of Tfh cell subsets during controlled human malaria infection ***A.*** *DEGs for each cluster were calculated at day 8, 16, and 36 compared to day 0. The number of DEGs for each subset and timepoint.* ***B.*** *Venn diagram indicating the shared and unique DEGS at day 16 for Tfh1_cytotoxic, Tfh1_CCR7 and Tfh2 subsets.* ***C.*** *Expression of activation genes MKI67, CD38 and ICOS at day 16 in each Tfh subset compared to Day 0.* ***D.*** *Expression of top 50 unique upregulated genes for Tfh1_Cyto, Tfh1_CCR7 and Tfh2 (curated from top 20 upregulated DEGs in Tfh1_CCR7, Tfh1_cytotoxic and Tfh2) cells across all three subsets at day 16 subsets. See also Supplementary Figure 6.*

Frequency and proliferation of malaria specific pTfh CCR7^{pos} cells is associated with the magnitude and function of antibody induction in CHMI

To confirm transcriptional findings at the phenotypic and antigen specific level and assess associations of different pTfh subsets with antibody induction, we assessed the activation of pTfh cells during CHMI in a subset of individuals from a previously published cohort (n= 19, sex 83.3%%

383 males, aged 24 years [20.2-28.2, median [IQR] years) *(10)*. Here we expanded on the published
384 analysis by focusing on malaria specific pTfh cells which were identified by Activated Induced
385 Marker (AIM) assays following PBMC stimulation with parasite infected RBCs (pRBCs)
386 *(14)* (**Supplementary Fig. 7A).** Consistent with scRNAseq analysis, AIM+ (CD69+OX40+) pTfh
387 cells were expanded at day 16 and 36 during CHMI. The frequencies of cells detected in control
388 stimulated cultures (uninfected RBCs) were unchanged (**Fig. 6A).** The largest response of malaria
389 specific (AIM+ in pRBC stim) pTfh cells occurred in pTfh1 CCR7^{pos} cells, however, increased
390 frequencies of Tfh1 CCR7^{neg} and Tfh2 cells were also detected, consistent with the proliferation and
391 expansion of these cells detected transcriptionally (**Fig. 6B**). Proliferation of AIM+ pTfh17 cells were
392 also detected at day 36 (p=0.051), however given that pTfh17 cells did not expand clonally, nor have
393 any detectable transcriptional changes during infection, these cells are likely to be TCR independent
394 cells which are activated via cytokines within AIM assays employed here *(43)*. Within malaria
395 specific pTfh1 CCR7^{pos}, pTfh1 CCR7^{neg} and pTfh2 cells, there were significant increases in
396 expression of activation markers ICOS and CD38, and proliferation marker Ki67 at day 16 and 36
397 (**Fig. 6C/D**). However, the expression of these markers was significantly higher on malaria specific
398 pTfh1 CCR7^{pos} cells compared to other subsets, consistent with the greatest expansion and activation
399 of pTfh1 CCR7^{pos} cells transcriptionally (**Fig. 6E/F**).

400 To investigate the link between each malaria specific pTfh cells and antibody development, we
401 correlated malaria-specific pTfh cells with antibodies produced after infection in response to intact
402 merozoites, quantified previously *(10)*. Antibody development was quantified with an antibody score
403 which captured the magnitude, breadth and functionality of response, by measuring IgM, IgG and IgG
404 subclasses, C1q fixation, FcR crosslinking and opsonic phagocytosis *(10)*. The frequencies of malaria-
405 specific pTfh1 CCR7^{pos}, pTfh1 CCR7^{neg} and pTfh2 cells correlated with each other, but not with
406 pTfh17 cells (**Fig. 6G)**. Despite this, pTfh1 CCR7^{pos} were correlated the most strongly and
407 consistently with antibody induction compared to other subsets, and were positively correlated with
408 total antibody score, and IgM and IgG to the merozoite (**Fig. 6G**), along with IgG1 and IgG2
409 (**Supplementary Fig. S7B).** In contrast, pTfh1 CCR7^{neg} cells only correlated with IgM and pTfh2
410 cells only correlated with antibody score (**Fig. 6G**). Similarly, while Ki67 expression amongst subsets
411 was correlated, only Ki67+ pTfh1 CCR7^{pos} and Ki67+ pTfh2 cells were correlated with antibody
412 score, IgG and IgM and antibody functions (**Fig. 6H, Supplementary Fig. S7D/E)**. Together, data
413 highlight that pTfh1 CCR7^{pos} and pTfh1 CCR7^{neg} cells have distinct functional potential. While both
414 are activated in malaria, pTfh1 CCR7^{pos} cells, together with pTfh2 cells, are more strongly associated
415 with antibody development.

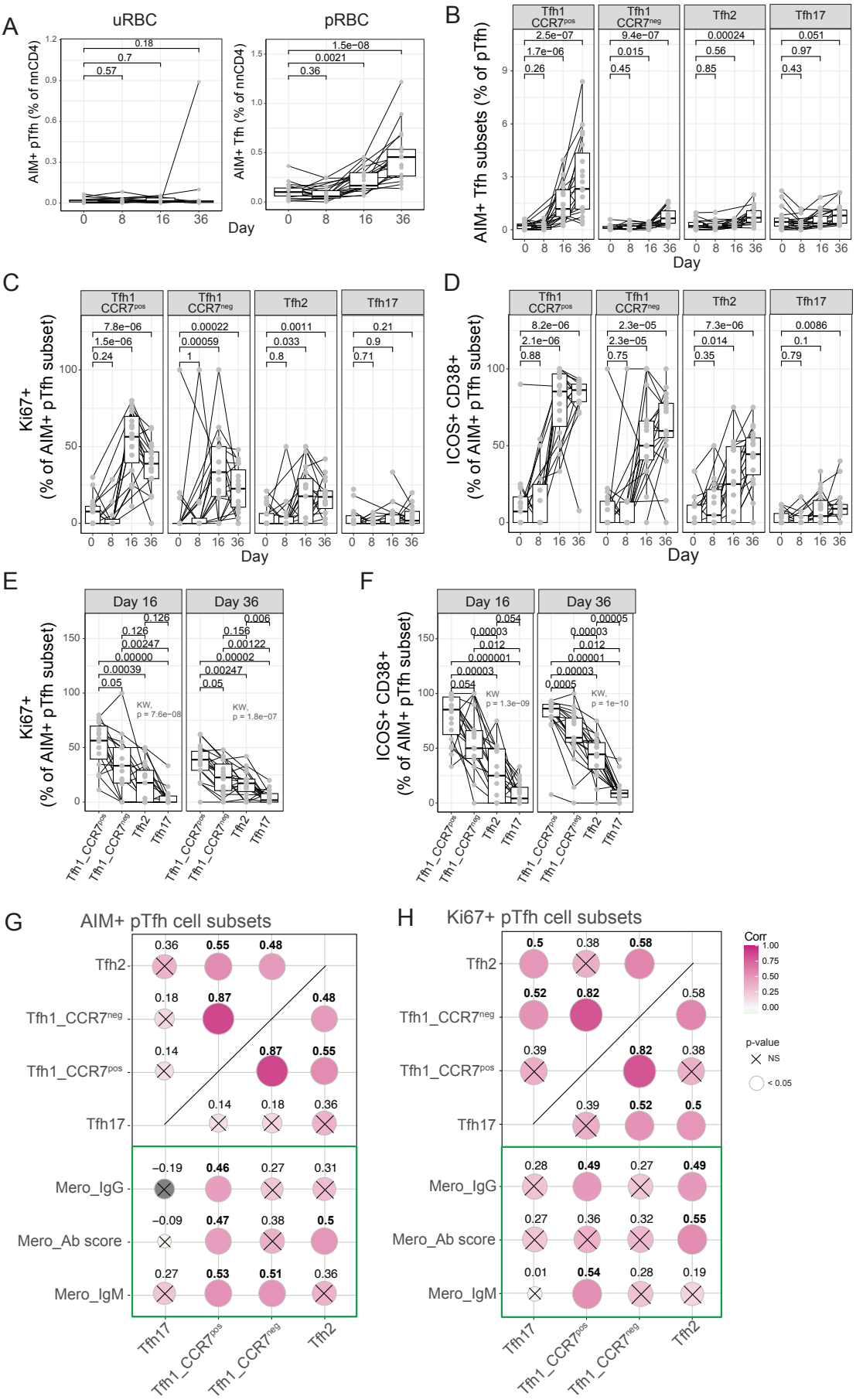
A
uRBC
pRBC
AIM+ pTfh (% of nnCD4)
AIM+ Tfh (% of nnCD4)
Day
B
Tfh1 CCR7pos
Tfh1 CCR7neg
Tfh2
Tfh17
AIM+ Tfh subsets (% of pTfh)
Day
C
Ki67+ (% of AIM+ pTfh subset)
Day
D
ICOS+ CD38+ (% of AIM+ pTfh subset)
Day
E
Day 16
Day 36
Ki67+ (% of AIM+ pTfh subset)
KW, p = 7.6e−08
KW, p = 1.8e−07
F
ICOS+ CD38+ (% of AIM+ pTfh subset)
KW p = 1.3e−09
KW, p = 1e−10
G
AIM+ pTfh cell subsets
Tfh2
Tfh1_CCR7neg
Tfh1_CCR7pos
Tfh17
Mero_IgG
Mero_Ab score
Mero_IgM
H
Ki67+ pTfh cell subsets
Corr
p-value
NS
< 0.05

416

417

418 ***Figure 6: Activation of malaria specific Tfh cells during malaria infection and association with***
419 ***antibody induction***

420 ***A.*** *Activation induced marker (AIM) assays were used to detected malaria specific pTfh cells in*
421 *individuals following CHMI (n= 15-20). AIM+ cells were identified as CD69+OX40+ pTfh cells after*
422 *stimulation with uninfected or parasite infected RBCs (uRBC and pRBC respectively) within all non-*
423 *naïve CD4 T cells. Malaria specific Tfh cells increased at day 16 and day 36 after infection.* ***B.***
424 *Malaria specific (AIM+) subset specific pTfh cells as a proportion of total pTfh cells.* ***C-D.*** *Ki67+ (C)*
425 *and ICOS+CD38+ (D) cells as a percentage of each AIM+ malaria specific pTfh subset during*
426 *CHMI comparing changes with infection.* ***E-F.*** *Ki67+ (E) and ICOS+CD38+ (F) cells as a*
427 *percentage of each AIM+ malaria specific pTfh subset at day 16, comparing expression levels*
428 *between subsets.* ***G-H.*** *Correlation between* ***(G)*** *malaria specific pTfh cell subsets or* ***(H)*** *Ki67*
429 *expression of Tfh subsets at day 36 with total IgG and IgM levels to merozoite, and overall antibody*
430 *score against merozoite, which captures the total antibody magnitude, breadth and functionality*
431 *specific to merozoite.* ***A-D****. P is the Wilcoxon rank-sum test for each infection timepoint against*
432 *baseline.* ***E-F****. P is the Wilcoxon rank-sum test after adjustment with multiple testing correction using*
433 *Holm's method, while the Kruskal-Wallis test is used for the global comparison.* ***G-H****. Spearman's*
434 *rho and p-value are indicated. See also Supplementary Figure 6 and Supplementary Figure 7.*

435

436 **Discussion**

437 Here we provide data that advances understanding of Tfh cell subsets, highlighting their functional
438 diversity across the course of human infection. Using unbiased analysis to integrate pTfh in the
439 resting state, we identify two clearly distinct pTfh1 subsets, which we show can be distinguished
440 based on CCR7 expression phenotypically. pTfh1 CCR7^{pos}cells have increased capacity to produce
441 IL-21, while cytotoxic markers are associated with pTfh1 CCR7^{neg} cells. Expanding our findings to
442 the context of human infection, we show during malaria that while pTfh1 CCR7^{pos}, pTfh1
443 cytotoxic/CCR7^{neg}, and Tfh2 cell subsets expand, and are activated, activation pathways are unique
444 between the subsets. We show both transcriptionally and at the malaria specific level, the magnitude
445 of activation is greatest in pTfh1 CCR7^{pos} cells, which also expand clonally. Additionally, the
446 frequency and proliferation of pTfh1 CCR7^{pos} cells was most consistently associated with antibody
447 induction compared to other subsets. Taken together, these findings provide new knowledge on Tfh
448 cell activation and functions during human infection. The specific role of pTfh1 CCR7^{pos} cells, but not
449 pTfh1 CCR7^{neg} responses in antibody induction during malaria resolves previously contradictory
450 findings on the potential roles of pTfh1-like subsets in the development of humoral immunity during
451 malaria.

452 Development of distinct Tfh cell subsets is suggested to be mediated by cytokine skewing driven by
453 distinct inflammatory milieu occurring during different immune responses to infection or vaccination
454 *(6)*. A recent investigation of Tfh cell development in mice immunized with Type-1 or Type-2
455 adjuvanted conditions supported this concept, inducing Tfh1 or Tfh2 cell-dominated responses,
456 respectively *(21)*. However, a comparative investigation of Tfh cell development and function in
457 different infections has highlighted that cytokine signalling within Tfh cells is more important in
458 driving subset fate than pathogen class *(22)*. For example, within that study Tfh cell fates induced by
459 LCMV and influenza, both of which drive type-1 immune responses, were distinct and drove differing
460 antibody responses *(22)*. While Tfh cells enriched for different cytokine signalling pathways could be
461 identified in human tonsils *(22)*, how distinct Tfh cell subsets develop in human infection is unclear.
462 Further, our data highlight that even within a single infection, induced pTfh cells are diverse. During
463 malaria infection both pTfh1 CCR7^{pos} and CCR7^{neg} subsets, along with pTfh2 are expanded,
464 transcriptionally activated and malaria specific. pTfh1 CCR7^{pos} cells shared clonal overlap with both
465 pTfh1 CCR7^{neg} cells and pTfh2 subsets, but these later subsets were largely clonally distinct from
466 each other. Shared clonal relationships of malaria specific pTfh1 and pTfh2 cells has been reported
467 previously *(44)*. Whether these relationships indicate cells along a single developmental pathway, or
468 divergence from a parent population and how cytokine signalling may influence subsets development
469 is unknown.

470 The importance of understanding Tfh cell subset development is highlighted by the distinct functional
471 consequences on antibody development linked to Tfh cell subset function. Human studies linking Tfh
472 cell subsets to antibody development have largely been limited to identifying Tfh cell subsets based
473 on CXCR3 and CCR6 expression *(4, 7, 8, 45)*, including in malaria *(10, 14–16, 44)*. Alternatively,
474 studies which include a more comprehensive analysis of pTfh cells have not related Tfh cell diversity
475 to antibody development *(34, 46)*. Here, our scRNAseq analysis shows that while CXCR3 and CCR6
476 are informative, diversity is masked by this gating strategy. Of functional relevance, within pTfh1-like
477 cells, we found that pTfh1 CCR7^{neg} cells contain the large majority of Tfh cells expressing cytotoxic
478 markers, including *NKG7,* granzyme K and granzyme B. In contrast, these markers were absent from
479 Tfh1 CCR7^{pos} cells, which produce comparatively higher levels of IL-21. Tfh cells with expression of
480 cytotoxic markers have been identified previously, and GC-Tfh cells which produce granzyme B in
481 response to group A *Streptococcus* kill B cells, potentially hampering antibody development *(36)*.
482 More recently granzyme K+ CMV specific pTfh cells were reported in humans. However, the
483 function of these cells in the context of antibody development is unknown *(21)*. During malaria
484 infection, we show that that while malaria specific pTfh1 CCR7^{pos}, pTfh1 CCR7^{neg} and pTfh2 cell
485 subsets are induced, only pTfh1 CCR7^{pos} and pTfh2 cell subsets were clearly associated with antibody
486 development. We have previously reported in the same cohort that global pTfh2 cell activation early
487 in infection (not considering antigen specificity) was associated with antibody development *(10)*.

488 While the importance of pTfh2 cells in antibody development to malaria has been supported by others
489 *(11–13)*, a negative role of pTfh1 in antibody development was difficult to rationalise in the context of
490 what is known from *in vitro* studies and animal models of induction of cytophilic IgG3 antibodies
491 which protect from malaria *(18)*. Data here resolve these contradictions with the identification of
492 distinct pTfh1 cell subsets. Further studies are required to investigate whether pTfh1 $CCR7^{neg}$ cells
493 with cytotoxic functions have negative roles in antibody induction, and how pTfh1 $CCR7^{pos}$ and
494 pTfh2 cells function to induce protective antibodies in malaria.

495 Limitations of our study include the analysis of pTfh cells isolated from peripheral blood of
496 volunteers, and not GC-Tfh within secondary lymphoid tissues. Future approaches to obtain and
497 analyse human secondary lymphoid tissue in the context of health and disease are needed. While pTfh
498 cells share overlapping signatures with GC-Tfh cells and are thought to provide a snapshot of the GC
499 response *(3)*, activated pTfh may not fully represent all GC-Tfh phenotypes and functions *(47)*. Future
500 studies will focus on developing approaches for fine needle aspirate studies of draining lymph nodes
501 during human malaria infection as applied to COVID and influenza vaccination settings *(23, 24, 47–*
502 *49)* , and investigating the immune response within the spleen in malaria infected individuals which is
503 likely a key site of antibody development in blood stage malaria *(50, 51)*. Nevertheless, such
504 approaches are not feasible for large human cohorts, thus data here on pTfh cells provides important
505 insights that can be applied to other human infection and vaccinations. Future studies dissecting
506 mechanisms of protective and disruptive Tfh cell development may lead to avenues to modulate Tfh
507 cells during infection or vaccination to induced more robust and protective antibody responses.

508 In conclusion, this study provides important new knowledge on functional diversity with pTfh cells
509 during human infection. The identification of further Tfh subsets and their potential functional
510 importance is highly relevant to developing novel therapeutics or new vaccine strategies that can
511 induce potent and long-lasting immunity against not only malaria, but other important pathogens.

512

513

514 **Materials and methods**

515 **Ethics statement**

516 Ethics approval for the use of human samples was obtained from the QIMR Berghofer Human
517 Research Ethics Committee (HREC P1479) and the Alfred Health Ethics Committee (288/23).
518 Written informed consent was obtained from all study participants.

519 **Study cohorts**

520 For CHMI studies, inoculum preparation, volunteer recruitment, infection, monitoring and treatment
521 were performed as previously described *(52)*. In brief, healthy malaria naive individuals underwent
522 CHMI with 2800 viable *P. falciparum* parasitized RBCs, and peripheral parasitaemia was measured at
523 least daily by qPCR as described previously *(53)*. Participants were treated with antimalarial drugs at
524 day 8 of infection when parasitaemia reaches approximately 20,000 parasites/ml. Blood samples
525 (from 5 studies across 6 independent cohorts) were collected prior to infection (day 0), at peak
526 infection (day 8) and 14 or 15 and 27-36 days (end of study, EOS) after inoculation (in analyses these
527 time points are grouped as 0, 8, 14/15 and EOS). PBMCs were isolated by Ficoll-Paque (Sigma,
528 USA) density gradient centrifugation, isolated PBMCs were cryopreserved in 10% DMSO/FBS.
529 Participants were healthy malaria naïve adults with no prior exposure to malaria or residence in
530 malaria-endemic regions. Clinical trials were registered at ClinicalTrials.gov NCT02867059 *(54)*,
531 NCT02783833 *(55)*, NCT02431637 *(56)*, and NCT02431650 *(56)*. For trials NCT02867059,
532 NCT02783833, NCT02431637 all participants received the same study drug (no-randomization) and
533 3D7-strain parasites. For NCT02431650, participants were randomized 1:1 to receive study drug
534 or control and 3D7-strain parasites. Samples used here were from samples opportunistically
535 collected from volunteers who consented to donate blood for immunological studies within the parent
536 clinical trial. As such, no sample size estimation was performed for this immunology study.

537 PBMCs from healthy non-infected controls was collected by the same processes for analysis of
538 responses following PMA/Io stimulation, development of transcriptional map of pTfh cells in health
539 donors.

540

541 **Ex vivo cell phenotyping with flow cytometry and activation induced marker assays**

542 PBMCs were thawed in RPMI 1640 (Gibco) containing 10% FCS and 0.02% Benzonase and rested
543 for 2 hours at 37°C, 5% CO2, and then cultured overnight in 96-well plates in 10% FCS/RPMI at 1 x
544 10^6 cells per well and stimulated for 18 hours with pRBCS or uninfected red blood cells (uRBCs) at
545 1:1 ratio. pRBC stimulated cells were used to assess malaria specific responses, and uRBC stimulated
546 cells were used to phenotype all Tfh cells. PBMCs were stained with antibodies against CD49b and
547 LAG-3 along with Fc block for 45 minutes at 37C, 5% CO_2. Following 2 washes with PBS, cells were
548 then stained with LIVE/DEAD Fixable Blue Dead Cell Stain for 15 minutes at room temperature,
549 washed twice with 2% FCS/PBS, and then surface stained for 15 minutes at room temperature with
550 fluorescent-tagged antibodies from Biolegend (CA, USA), and BD Biosciences (CA, USA)
551 (**Supplementary Table S3**) e. After 2 washes with 2% FCS/PBS Cells were fixed and permeabilized
552 with eBioscienceTM Foxp3 / Transcription Factor Staining Buffer Set (Thermo Fisher Scientific
553 (MA, USA); Cat. #00-5523-00) solution for 20 minutes on ice. After 2 washes with 1X perm buffer,
554 intracellular staining was performed for 30 minutes on ice with fluorescent-tagged antibodies from

555 Biolegend (CA, USA), and BD Biosciences (CA, USA) (**Supplementary Table S3**). Cells were re-
556 suspended in 2% FCS/PBS, and events were collected on the Cytek Aurora 5 laser cytometer (CA,
557 USA).

558 **PMA stimulation and intracellular cytokine staining**

559 Approximately 1 x 10^6 PBMCs were used per patient per condition/ stain. Thawing of cryopreserved
560 PBMCs was done as previously described. For cytokine induction following PMA and Ionomycin
561 stimulation, PBMC samples were rested overnight in 10% FCS/RPMI after thawing. After rest,
562 PBMCs were stimulated with PMA (25 ng/ mL; Sigma) and Ionomycin (1 ug/mL; Sigma) for 6 hours
563 at 37°C, 5% CO2. Brefeldin A (10 ug/mL; BD Biosciences) and monensin (10 ug/mL; BD
564 Biosciences) were added after the first 2 hours of stimulation. To account for downregulation of
565 chemokine receptors after exposure to BFA and monensin, antibodies against CCR7, CXCR3,
566 CXCR5 and CCR6 were added alongside Fc block during stimulation with PMA/Ionomycin, prior to
567 addition of BFA and monensin. Anti-CD107a was also included during stimulation for intracellular
568 capture. After stimulation, cells were washed with PBS and stained at room temperature for
569 15 minutes with LIVE/DEAD Fixable Blue Dead Cell Stain, washed twice with 2% FCS/PBS, and
570 then surface stained with the antibodies listed in **Supplementary Table S4** for 15 minutes at room
571 temperature. Following 2 washes with 2% FCS/PBS, cells underwent fixation/permeabilization with
572 eBioscience Fixation/Permeabilization solution for 20 minutes on ice and washed in permeabilization
573 buffer. Intracellular staining (ICS) with the antibodies listed in **Supplementary Table S4** was
574 performed for 30 minutes on ice following washes with permeabilization buffer and then fixed with
575 BD stabilizing fixative. Samples were acquired on Cytek Aurora 5.

576 **Flow cytometry data analysis**

577 Flow cytometry data was analysed using FlowJo v10 and then analysed on R (version 4.4.2). For
578 unsupervised data analysis, spectre (version 1.2.0) was used *(57)*.

579

580 **Single Cell RNA sequencing and analysis**

581 *Cell isolation*

582

583 <u>Healthy reference data set –</u> PBMCs from four healthy donors were thawed in thawed in RPMI 1640
584 (Gibco) containing 10% FCS and 0.02% Benzonase. Cells were rested for 2 hours in 10% FCS/PBS at
585 37C, 5% CO_2. After rest, untouched CD4+ T cells were enriched from PBMCs using the CD4+ T cell
586 isolation kit (Miltenyi). Enriched CD4+ T cells were then incubated with Fc block for 15 minutes and
587 then surface stained with antibodies listed in **Supplementary Table S8** for 15 minutes at room
588 temperature. Cells were washed with 0.5% BSA/PBS and stained for viability with Sytox Blue

589 (Invitrogen (CA, USA), Cat. # S34857) and sorted on BD FACSAria™III Cell Sorter into 0.5%
590 BSA/PBS. Four populations of cells were sorted, PD1- Tfh (nnCD4/CXCR5+/PD1-), pTfh1
591 (nnCD4/CXCR5+/PD1+/CXCR3+ CCR6-), pTfh2 (nnCD4/CXCR5+/PD1+/CXCR3- CCR6-) and
592 pTfh17 (nnCD4/CXCR5+/PD1+/CXCR3- CCR6+). After sorting, cells of a single phenotype were
593 pooled and run on a single 10X Chromium lane.
594
595 CHMI – PBMCs collected at day 0, 8, 16, 36 from four participants in CHMI study NCT02867059
596 *(54)* were thawed in RPMI 1640 (Gibco) containing 10% FCS and 0.02% Benzonase. Cells were
597 washed with 0.5% BSA/PBS and then incubated with Fc block and antibodies against pan-gD and
598 CXCR5 for 15 minutes at room temperature. Following that, the other antibodies listed in Stain 2 in
599 **Supplementary Table S9** were added and cells were incubated for another 15 minutes at room
600 temperature. Cells were washed and stained for viability with Sytox Blue (Invitrogen (CA, USA), Cat.
601 # S34857) and sorted on BD FACSAria™III Cell Sorter into 0.5% BSA/PBS. Live Tfh cells were
602 sorted as nnCD4, CXCR5+PD1+ cells. After sorting, cells from a single time point were pooled and
603 run on a single 10X Chromium lane.
604
605 *10 X Genomics Chromium GEX Library preparation and sequencing*

606 Sorted cells were loaded into each lane of Chromium Next GEM Single Cell 5' Reagent Kit v2 and
607 Gel Bead-in- Emulsion (GEMs) generated in the 10X Chromium Controller (Chromium Next GEM
608 Single Cell 5' Kit v2, PN-1000263, Chromium Single cell V(D)J Amplification Kits: Human TCR,
609 PN-1000252, Chromium Next GEM Chip K Single Cell Kit, PN-1000286, , Dual Index Kit TT Set
610 A, PN-1000215). 5' Gene Expression
611 Libraries and VDJ libraries (TCR) were generated according to the manufacturer's instructions.
612 Generated libraries were sequenced in a NextSeq 550 System using High Output Kit (150 Cycles)
613 version 1 according to the manufacturer's protocol using paired-end sequencing (150-bp Read 1 and
614 150 bp Read 2) with the following parameters Read 1: 26 cycles, i7 index: 10 cycles, i5 index: 10
615 cycles and Read 2: 90 cycles.
616
617 *Demultiplexing and analysis*

618 ScRNAseq data was demultiplexed, aligned and quantified using Cell Ranger version 3.1.0 software
619 (10x Genomics) against the human reference genome (GRCh38-3.0.0) with default parameters. Cell
620 genotype was obtained using cellsnp-lite *(58)* with the list of informative SNPs obtained from
621 1000_Genome_Project *(59)*. Then vireo was used to predict the original donor utilising the cell's
622 haplotype ratios, only predicted singlets were used for the analysis *(60)*. Cell ranger count matrices for
623 each sample were loaded, merged and analysed using Seurat package v4.3.0 and v5.1.0 *(61)* and
624 visualised with scCustomize v3.0.1 *(62)*. The healthy reference and CHMI datasets were processed as

625 two separate datasets. Cells were filtered to remove those expressing fewer than 200 genes and more
626 than 4000 genes, and those with more than 10% mitochondrial content. Only genes expressed in three
627 or more cells were considered. TRA/TRB gene expression were removed from the GEX dataset prior
628 to further downstream processing.
629
630 For Healthy Reference map – Dataset was split by donor and then each individual donor dataset was
631 normalised with SCTransform where highly variable genes were also selected. Before integration, the
632 most variable genes shared among the donor datasets were identified using FindintegrationAnchors
633 and were used to integrate the datasets using the IntegrateData function. Following that, PCA
634 dimensionality reduction was performed using RunPCA and the top 20 PCs were used to compute
635 UMAP visualisation using RunUMAP.
636
637 For CHMI data - Dataset was split per donor and day, then each individual donor_day dataset was
638 normalised with SCTransform where highly variable genes were also selected.*(63)* Before integration,
639 the most variable genes shared among the datasets were identified using FindIntegrationAnchors and
640 used to integrate the datasets using the IntegrateData function. Following that, PCA dimensionality
641 reduction was performed using RunPCA and the top 20 PCs were used to compute UMAP
642 visualisation using RunUMAP.
643
644 *Cell cluster annotation*
645 Healthy reference map – We applied unsupervised clustering using the Louvain algorithm as our
646 modularity optimisation technique and set the granularity of clusters at a resolution of 0.3. A cluster
647 with high mitochondrial content and low read counts was removed as it implies a cluster of cells of
648 low quality. RNA-level counts were log-normalised using NormalizeData (scale factor = 10,000 by
649 default) and were used to run FindMarkers for identifying cluster marker genes as part of cluster
650 annotation. This identified the Tfh1 cluster, along with Tfh2, Tfh17 stress, ribosomal, Type I IFN,
651 cluster 2 and cluster 3 clusters. We then visualised the expression of Treg-related genes (*FOXP3* and
652 *IL2RA)* on the map to identify a cluster of cells belonging to Tfreg within Tfh2 cluster, and another
653 subset of Tfh1/17 cluster which expressed *RORC* along with *CXCR3*, that were positioned separately
654 from the main Tfh1 cluster. Further sub-clustering was also attempted on each of the main Tfh1/2/17
655 clusters separately to identify any higher-level annotations/groupings that could exist within each
656 subset, however only 2 sub-clusters within the Tfh1 subset were suggested to be of functional
657 difference. Automated cell labelling tool, scType *(40)*, was used to transfer labels from the healthy
658 reference Tfh map onto a published human tonsil Tfh dataset *(29)* containing non-GC and GC Tfh
659 subsets. Detailed steps of how the label transfer was performed is as per described below in CHMI
660 data section. Cluster markers of each cluster were further analysed for pathway enrichment using the
661 Ingenuity Pathway Analysis (IPA) suite (v01-22-01, QIAGEN, DUS, Germany).

662 CHMI data – Unsupervised clustering was calculated using Louvain algorithm with resolution set at
663 2.2 to achieve overclustering. Low-quality clusters with high mitochondrial content and low read
664 counts were removed. Label transfer using cell type annotations from the Healthy Reference Map
665 onto the CMHI dataset was performed using scType *(40)*. The top 20 up- and down-regulated cluster
666 marker genes from each reference cell type were used to calculate a specificity score to predict the
667 cell type for each cluster in the CHMI dataset. Based on the final top-specificity score, similar clusters
668 are then stitched together for the final annotation. As an additional quality check step, a fold-change
669 between the score of the top-predicted cell type versus every other possible cell type was calculated
670 per cluster, and any cluster where the difference between the top-predicted cell type and the next
671 possible cell type was less than 1.1 was flagged as "low confidence". For clusters 14, 19 and 22 where
672 the top-predicted cell type was flagged as "low-confidence", a manual comparison of key cell type
673 marker genes was done to confirm the final cell annotation used (final annotation: cluster 14 as
674 Tfh1_CCR7, cluster 19 as cluster 2, cluster 22 as Tfh1_Cyto). After the final prediction, we visualised
675 Treg markers (*"Il2ra", "Foxp3"*) and manually selected for an area on the UMAP with high
676 expression of these markers as "Tfr" cluster. For the reference database, we omitted Tfh1/17 and Tfr
677 as input as these 2 clusters had signatures commonly shared with the other clusters: Tfh1/17 with
678 Tfh1 and Tfh17, and Tfreg with Tfh2. RNA-level counts were log-normalised using NormalizeData
679 (scale factor = 10,000 by default) and were used to run FindMarkers for identifying additional cluster
680 marker genes for each annotated cluster.

681 *Pseudobulked Differential Gene Expression Analysis and Pathway Analysis*

682 The normalised count matrix and the metadata were extracted from the Seurat object. Counts were
683 aggregated per sample (i.e. donor and day) for each cluster. Since we conducted a paired-wise
684 comparison (e.g. day 0 vs day 16) only clusters present in both samples were included in the analysis.
685 Significant genes were determined using the quasi-likelihood (QL) F-test with an FDR< 0.05 using
686 edgeR *(64)*. Aggregated counts were used for visualising changes in specific DEGs using
687 ComplexHeatmap.

688 *TCRA/B clonal analysis*

689 Annotated TCR sequences were integrated with the single-cell transcriptomics data using the
690 combineTCR and combineExpression functions from scRepertoire (version 2.0.0). The CDR3 amino
691 acid sequences were used to call and quantify clones. Only cells with single and complete paired TCRA
692 and TCRB chain were included. The R package circlize (v0.4.16) and clonalOverlap function of
693 scRepertoire were used to generate the circos and heatmap plots of clonal overlap, respectively. For
694 Simpson's diversity index calculations, data were down-sampled to 1,000 cells to adjust for cell count
695 variations between samples.

696

697 **Statistical analysis**

698 Non-parametric testing was performed for all analysis. Continuous data for all cellular responses were
699 compared between groups using Mann-Whitney U test, or in paired samples with Wilxcox paired
700 sign-rank test, or correlated with antibody score as a continuous variable with Spearman's
701 correlations. Statistical comparisons were adjusted for multiple comparisons where indicated. All
702 analyses were performed in R (version 4.4.2). Graphical outputs were made in ggplot2 (version 3.5.1)
703 and ggpubr (version 0.6.0). No sample size calculation was performed, instead all available
704 participant data was included. Due to sample size restrictions, no subgroup analysis was performed.
705 Data generation was performed with blinding to participant demographic data.

706

707 **Data and code availability**

708 All data generated or analysed during this study are included in this article and supplementary
709 information files or deposited online as follows. The raw sequencing data and processed Cell Ranger
710 outputs used in this study have been deposited in the NCBI data base under accession code
711 GSE272939 https://www.ncbi.nlm.nih.gov/geo/query/acc.cgi?acc=GSE272939 and GSE253661
712 https://www.ncbi.nlm.nih.gov/geo/query/acc.cgi?acc=GSE253661.

713 The processed single cell RNA sequencing data are available in the Zenodo,
714 https://doi.org/10.5281/zenodo.14847353.

715 Code used to analyse scRNAseq data is available at https://github.com/MichelleBoyle/CCR7-
716 expression-defines-distinct-pTfh1-subsets-involved-in-malaria-immunity.git

717 Flow cytometry files will be made freely available on publication in an online repository.

718

719

720 **Author contributions**

721 MSFS, ND, RM, DA, JRL and JAC generated data, supervised by JGB, CE, AH and MJB

722 MSFS, DAO, ZP analysed data

723 JM and BB provided clinical samples used in this study

724 AH and MJB conceptualised study

725 MSFS and MJB led manuscript writing.
726 All authors contributed to and approved manuscript

727 **Declarations of interest**

728 All authors declare no conflicts of interest

729 **Acknowledgements**

730 Burnet Institute, University of Melbourne and QIMR-Berghofer acknowledge the traditional
731 custodians of the lands where they are located, the Boonwurrung and Wurundjeri Woi-wurrong
732 people of the Kulin Nation, and the Turrbal and Jagera people.

733 RBC and human serum were provided by the Australian Red Cross Blood Bank (Melbourne and
734 Brisbane). We thank the participants involved in the CHMI studies and all study clinicians and
735 support staff at QPharm.

736 This work was supported by the National Health and Medical Research Council of Australia (program
737 grant 1132975 to J.S.M and C.R.E.); Senior Research Fellowships C.R.E. (1154265), Career
738 Development Award 1141278, Project Grant 1125656, and Ideas Grant 1181932 to MJB.; Emerging
739 Leadership 2 Fellowship 2016792 to BEB); the CSL Centenary Fellowship and the Snow Medical
740 Foundation Fellowship 2022/SF167 to M.J.B; the Jim and Margaret Beever Fellowship to J.A.C. The
741 Burnet Institute is supported by the NHMRC for Independent Research Institutes Infrastructure
742 Support Scheme and the Victorian State Government Operational Infrastructure Support. Medicines
743 for Malaria Venture funded the parent CHMI studies.

744

745

746

747 **References**

748

749 1. D. Yu, L. S. K. Walker, Z. Liu, M. A. Linterman, Z. Li, Targeting TFH cells in human
750 diseases and vaccination: rationale and practice. *Nat. Immunol.* **23**, 1157–1168 (2022).

751 2. E. Brenna, A. N. Davydov, K. Ladell, J. E. McLaren, P. Bonaiuti, M. Metsger, J. D.
752 Ramsden, S. C. Gilbert, T. Lambe, D. A. Price, S. L. Campion, D. M. Chudakov, P. Borrow,
753 A. J. McMichael, CD4+ T Follicular Helper Cells in Human Tonsils and Blood Are Clonally
754 Convergent but Divergent from Non-Tfh CD4+ Cells. *CellReports* **30**, 137-152.e5 (2020).

755 3. L. A. Vella, M. Buggert, S. Manne, R. S. Herati, I. Sayin, L. Kuri-Cervantes, I. B. Brody,
756 K. C. O'Boyle, H. Kaprielian, J. R. Giles, S. Nguyen, A. Muselman, J. P. Antel, A. Bar-Or,
757 M. E. Johnson, D. H. Canaday, A. Naji, V. V. Ganusov, T. M. Laufer, A. D. Wells, Y. Dori,
758 M. G. Itkin, M. R. Betts, E. J. Wherry, T follicular helper cells in human efferent lymph
759 retain lymphoid characteristics. *The Journal of clinical investigation* **129**, 3185–3200 (2019).

760 4. R. Morita, N. Schmitt, S.-E. Bentebibel, R. Ranganathan, L. Bourdery, G. Zurawski, E.
761 Foucat, M. Dullaers, S. Oh, N. Sabzghabaei, E. M. Lavecchio, M. Punaro, V. Pascual, J.
762 Banchereau, H. Ueno, Human blood CXCR5(+)CD4(+) T cells are counterparts of T
763 follicular cells and contain specific subsets that differentially support antibody secretion.
764 *Immunity* **34**, 108–121 (2011).

765 5. A. Heit, F. Schmitz, S. Gerdts, B. Flach, M. S. Moore, J. A. Perkins, H. S. Robins, A.
766 Aderem, P. Spearman, G. D. Tomaras, S. C. D. Rosa, M. J. McElrath, Vaccination
767 establishes clonal relatives of germinal center T cells in the blood of humans. *The Journal of*
768 *experimental medicine* **214**, 2139–2152 (2017).

769 6. A. C. Olatunde, J. S. Hale, T. J. Lamb, Cytokine-skewed Tfh cells: functional
770 consequences for B cell help. *Trends Immunol.* **42**, 536–550 (2021).

771 7. M. Locci, C. Havenar-Daughton, E. Landais, J. Wu, M. A. Kroenke, C. L. Arlehamn, L. F.
772 Su, R. Cubas, M. M. Davis, A. Sette, E. K. Haddad, P. Poignard, S. Crotty, Human
773 Circulating PD-1+CXCR3-CXCR5+ Memory Tfh Cells Are Highly Functional and Correlate
774 with Broadly Neutralizing HIV Antibody Responses. *Immunity* **39**, 758–769 (2013).

775 8. S.-E. Bentebibel, S. Lopez, G. Obermoser, N. Schmitt, C. Mueller, C. Harrod, E. Flano, A.
776 Mejias, R. A. Albrecht, D. Blankenship, H. Xu, V. Pascual, J. Banchereau, A. Garcia-Sastre,
777 A. K. Palucka, O. Ramilo, H. Ueno, Induction of ICOS+CXCR3+CXCR5+ TH Cells
778 Correlates with Antibody Responses to Influenza Vaccination. *Sci. Transl. Med.* **5**, 176ra32
779 (2013).

780 9. S.-E. Bentebibel, S. Khurana, N. Schmitt, P. Kurup, C. Mueller, G. Obermoser, A. K.
781 Palucka, R. A. Albrecht, A. Garcia-Sastre, H. Golding, H. Ueno, ICOS+PD-1+CXCR3+ T
782 follicular helper cells contribute to the generation of high-avidity antibodies following
783 influenza vaccination. *Sci. Rep.* **6**, 26494 (2016).

784 10. J.-A. Chan, J. R. Loughland, F. de L. Rivera, A. SheelaNair, D. W. Andrew, N. L.
785 Dooley, B. D. Wines, F. H. Amante, L. Webb, P. M. Hogarth, J. S. McCarthy, J. G. Beeson,

786 C. R. Engwerda, M. J. Boyle, Th2-like T Follicular Helper Cells Promote Functional
787 Antibody Production during Plasmodium falciparum Infection. *Cell Reports Medicine* **1**,
788 100157 (2020).

789 11. G. Bowyer, A. Grobbelaar, T. Rampling, N. Venkatraman, D. Morelle, R. W. Ballou, A.
790 V. S. Hill, K. J. Ewer, CXCR3+ T Follicular Helper Cells Induced by Co-Administration of
791 RTS,S/AS01B and Viral-Vectored Vaccines Are Associated With Reduced Immunogenicity
792 and Efficacy Against Malaria. *Front Immunol* **9**, 1660 (2018).

793 12. C. M. Nielsen, A. Ogbe, I. Pedroza-Pacheco, S. E. Doeleman, Y. Chen, S. E. Silk, J. R.
794 Barrett, S. C. Elias, K. Miura, A. Diouf, M. Bardelli, R. A. Dabbs, L. Barfod, C. A. Long, B.
795 F. Haynes, R. O. Payne, A. M. Minassian, T. Bradley, S. J. Draper, P. Borrow,
796 Protein/AS01B vaccination elicits stronger, more Th2-skewed antigen-specific human T
797 follicular helper cell responses than heterologous viral vectors. *Cell Reports Medicine* ,
798 100207 (2021).

799 13. A. M. Minassian, S. E. Silk, J. R. Barrett, C. M. Nielsen, K. Miura, A. Diouf, C. Loos, J.
800 K. Fallon, A. R. Michell, M. T. White, N. J. Edwards, I. D. Poulton, C. H. Mitton, R. O.
801 Payne, M. Marks, H. Maxwell-Scott, A. Querol-Rubiera, K. Bisnauthsing, R. Batra, T.
802 Ogrina, N. J. Brendish, Y. Themistocleous, T. A. Rawlinson, K. J. Ellis, D. Quinkert, M.
803 Baker, R. L. Ramon, F. R. Lopez, L. Barfod, P. M. Folegatti, D. Silman, M. Datoo, I. J.
804 Taylor, J. Jin, D. Pulido, A. D. Douglas, W. A. de Jongh, R. Smith, E. Berrie, A. R. Noe, C.
805 L. Diggs, L. A. Soisson, R. Ashfield, S. N. Faust, A. L. Goodman, A. M. Lawrie, F. L.
806 Nugent, G. Alter, C. A. Long, S. J. Draper, Reduced blood-stage malaria growth and immune
807 correlates in humans following RH5 vaccination. *Med* **2**, 701-719.e19 (2021).

808 14. Damian. A. Oyong, Jessica. R. Loughland, Megan. S. F. Soon, J.-A. Chan, D. Andrew, B.
809 D. Wines, P. M. Hogarth, S. D. Olver, A. D. Collinge, A. Varelias, J. G. Beeson, E.
810 Kenangalem, R. N. Price, N. M. Anstey, G. Minigo, M. J. Boyle, Adults with Plasmodium
811 falciparum malaria have higher magnitude and quality of circulating T-follicular helper cells
812 compared to children. *Ebiomedicine* **75**, 103784 (2022).

813 15. N. Obeng-Adjei, S. Portugal, T. M. Tran, T. B. Yazew, J. Skinner, S. Li, A. Jain, P. L.
814 Felgner, O. K. Doumbo, K. Kayentao, A. Ongoiba, B. Traore, P. D. Crompton, Circulating
815 Th1-Cell-type Tfh Cells that Exhibit Impaired B Cell Help Are Preferentially Activated
816 during Acute Malaria in Children. *CellReports* **13**, 425–439 (2015).

817 16. J.-A. Chan, J. R. Loughland, L. de la Parte, S. Okano, I. Ssewanyana, M. Nalubega, F.
818 Nankya, K. Musinguzi, J. Rek, E. Arinaitwe, P. Tipping, P. Bourke, D. Andrew, N. Dooley,
819 A. SheelaNair, B. D. Wines, P. M. Hogarth, J. G. Beeson, B. Greenhouse, G. Dorsey, M.
820 Kamya, G. Hartel, G. Minigo, M. Feeney, P. Jagannathan, M. J. Boyle, Age-dependent
821 changes in circulating Tfh cells influence development of functional malaria antibodies in
822 children. *Nat Commun* **13**, 4159 (2022).

823 17. N. Obeng-Adjei, S. Portugal, P. Holla, S. Li, H. Sohn, A. Ambegaonkar, J. Skinner, G.
824 Bowyer, O. K. Doumbo, B. Traore, S. K. Pierce, P. D. Crompton, C. R. Engwerda, Ed.
825 Malaria-induced interferon-γ drives the expansion of Tbethi atypical memory B cells. *PLoS*
826 *pathogens* **13**, e1006576 (2017).

827 18. D. H. Opi, L. Kurtovic, J.-A. Chan, J. L. Horton, G. Feng, J. G. Beeson, Multi-functional
828 antibody profiling for malaria vaccine development and evaluation. *Expert Rev Vaccines* **20**,
829 1257–1272 (2021).

830 19. A. Ly, Y. Liao, H. Pietrzak, L. J. Ioannidis, T. Sidwell, R. Gloury, M. Doerflinger, T.
831 Triglia, R. Z. Qin, J. R. Groom, G. T. Belz, K. L. Good-Jacobson, W. Shi, A. Kallies, D. S.
832 Hansen, Transcription Factor T-bet in B Cells Modulates Germinal Center Polarization and
833 Antibody Affinity Maturation in Response to Malaria. *Cell Reports* **29**, 2257-2269.e6 (2019).

834 20. J. J. Guthmiller, A. C. Graham, R. A. Zander, R. L. Pope, N. S. Butler, Cutting Edge: IL-
835 10 Is Essential for the Generation of Germinal Center B Cell Responses and Anti-
836 Plasmodium Humoral Immunity. *J Immunol* **198**, 617–622 (2017).

837 21. S. Kumar, A. P. Basto, F. Ribeiro, S. C. P. Almeida, P. Campos, C. Peres, N. Pulvirenti,
838 S. Al-Khalidi, A. Kilbey, J. Tosello, E. Piaggio, M. Russo, M. Gama-Carvalho, S. B. Coffelt,
839 E. W. Roberts, J. Geginat, H. F. Florindo, L. Graca, Specialized Tfh cell subsets driving type-
840 1 and type-2 humoral responses in lymphoid tissue. *Cell Discov.* **10**, 64 (2024).

841 22. L. Dalit, C. W. Tan, A. A. Sheikh, R. Munnings, C. Alvarado, T. Hussain, A. Zaini, L.
842 Cooper, A. Kirn, L. Hailes, A. Nguyen, L. Mackay, N. Harris, C. Zaph, N. L. L. Gruta, S. L.
843 Nutt, K. Good-Jacobson, M. J. Davis, V. L. Bryant, J. R. Groom, Divergent cytokine and
844 transcriptional signatures control functional T follicular helper cell heterogeneity. (2024),
845 doi:10.1101/2024.06.12.598622.

846 23. N. Borcherding, W. Kim, M. Quinn, F. Han, J. Q. Zhou, A. J. Sturtz, A. J. Schmitz, T.
847 Lei, S. A. Schattgen, M. K. Klebert, T. Suessen, W. D. Middleton, C. W. Goss, C. Liu, J. C.
848 Crawford, P. G. Thomas, S. A. Teefey, R. M. Presti, J. A. O'Halloran, J. S. Turner, A. H.
849 Ellebedy, P. A. Mudd, CD4+ T cells exhibit distinct transcriptional phenotypes in the lymph
850 nodes and blood following mRNA vaccination in humans. *Nat. Immunol.* , 1–11 (2024).

851 24. S. A. Schattgen, J. S. Turner, M. A. Ghonim, J. C. Crawford, A. J. Schmitz, H. Kim, J. Q.
852 Zhou, W. Awad, R. C. Mettelman, W. Kim, K. M. McIntire, A. Haile, M. K. Klebert, T.
853 Suessen, W. D. Middleton, S. A. Teefey, R. M. Presti, A. H. Ellebedy, P. G. Thomas,
854 Influenza vaccination stimulates maturation of the human T follicular helper cell response.
855 *Nat. Immunol.* , 1–12 (2024).

856 25. W. Xu, X. Zhao, X. Wang, H. Feng, M. Gou, W. Jin, X. Wang, X. Liu, C. Dong, The
857 Transcription Factor Tox2 Drives T Follicular Helper Cell Development via Regulating
858 Chromatin Accessibility. *Immunity* **51**, 826-839.e5 (2019).

859 26. S. Horiuchi, H. Wu, W.-C. Liu, N. Schmitt, J. Provot, Y. Liu, S.-E. Bentebibel, R. A.
860 Albrecht, M. Schotsaert, C. V. Forst, B. Zhang, H. Ueno, Tox2 is required for the
861 maintenance of GC TFH cells and the generation of memory TFH cells. *Sci Adv* **7**, eabj1249
862 (2021).

863 27. M. A. Kroenke, D. Eto, M. Locci, M. Cho, T. Davidson, E. K. Haddad, S. Crotty, Bcl6
864 and Maf Cooperate To Instruct Human Follicular Helper CD4 T Cell Differentiation. *J.
865 Immunol.* **188**, 3734–3744 (2012).

28. F. Andris, S. Denanglaire, M. Anciaux, M. Hercor, H. Hussein, O. Leo, The Transcription Factor c-Maf Promotes the Differentiation of Follicular Helper T Cells. *Front. Immunol.* **8**, 480 (2017).

29. R. Massoni-Badosa, S. Aguilar-Fernández, J. C. Nieto, P. Soler-Vila, M. Elosua-Bayes, D. Marchese, M. Kulis, A. Vilas-Zornoza, M. M. Bühler, S. Rashmi, C. Alsinet, G. Caratù, C. Moutinho, S. Ruiz, P. Lorden, G. Lunazzi, D. Colomer, G. Frigola, W. Blevins, L. Romero-Rivero, V. Jiménez-Martínez, A. Vidal, J. Mateos-Jaimez, A. Maiques-Diaz, S. Ovejero, J. Moreaux, S. Palomino, D. Gomez-Cabrero, X. Agirre, M. A. Weniger, H. W. King, L. C. Garner, F. Marini, F. J. Cervera-Paz, P. M. Baptista, I. Vilaseca, C. Rosales, S. Ruiz-Gaspà, B. Talks, K. Sidhpura, A. Pascual-Reguant, A. E. Hauser, M. Haniffa, F. Prosper, R. Küppers, I. G. Gut, E. Campo, J. I. Martin-Subero, H. Heyn, An atlas of cells in the human tonsil. *Immunity* (2024), doi:10.1016/j.immuni.2024.01.006.

30. M. E. Cook, I. Shchukina, C.-C. Lin, T. R. Bradstreet, E. A. Schwarzkopf, N. N. Jarjour, A. M. Webber, K. Zaitsev, M. N. Artyomov, B. T. Edelson, BHLHE40 Mediates Cross-Talk between Pathogenic TH17 Cells and Myeloid Cells during Experimental Autoimmune Encephalomyelitis. *ImmunoHorizons* **7**, 737–746 (2023).

31. C.-C. Lin, T. R. Bradstreet, E. A. Schwarzkopf, N. N. Jarjour, C. Chou, A. S. Archambault, J. Sim, B. H. Zinselmeyer, J. A. Carrero, G. F. Wu, R. Taneja, M. N. Artyomov, J. H. Russell, B. T. Edelson, IL-1–induced Bhlhe40 identifies pathogenic T helper cells in a model of autoimmune neuroinflammation. *J. Exp. Med.* **213**, 251–271 (2016).

32. R. D. Hatton, TGF-β in Th17 Cell Development: The Truth Is Out There. *Immunity* **34**, 288–290 (2011).

33. M. M. Xie, S. Fang, Q. Chen, H. Liu, J. Wan, A. L. Dent, Follicular regulatory T cells inhibit the development of granzyme B-expressing follicular helper T cells. *JCI insight* **4** (2019), doi:10.1172/jci.insight.128076.

34. C. Liang, S. Spoerl, Y. Xiao, K. M. Habenicht, S. S. Haeusl, I. Sandner, J. Winkler, N. Strieder, R. Eder, H. Stanewsky, C. Alexiou, D. Dudziak, A. Rosenwald, M. Edinger, M. Rehli, P. Hoffmann, T. H. Winkler, F. Berberich-Siebelt, Oligoclonal CD4+CXCR5+ T cells with a cytotoxic phenotype appear in tonsils and blood. *Commun. Biol.* **7**, 879 (2024).

35. J. He, L. M. Tsai, Y. A. Leong, X. Hu, C. S. Ma, N. Chevalier, X. Sun, K. Vandenberg, S. Rockman, Y. Ding, L. Zhu, W. Wei, C. Wang, A. Karnowski, G. T. Belz, J. R. Ghali, M. C. Cook, D. S. Riminton, A. Veillette, P. L. Schwartzberg, F. Mackay, R. Brink, S. G. Tangye, C. G. Vinuesa, C. R. Mackay, Z. Li, D. Yu, Circulating Precursor CCR7loPD-1hi CXCR5+ CD4+ T Cells Indicate Tfh Cell Activity and Promote Antibody Responses upon Antigen Reexposure. *Immunity* **39**, 770–781 (2013).

36. J. M. Dan, C. Havenar-Daughton, K. Kendric, R. Al-Kolla, K. Kaushik, S. L. Rosales, E. L. Anderson, C. N. LaRock, P. Vijayanand, G. Seumois, D. Layfield, R. I. Cutress, C. H. Ottensmeier, C. S. L. Arlehamn, A. Sette, V. Nizet, M. Bothwell, M. Brigger, S. Crotty, Recurrent group A Streptococcus tonsillitis is an immunosusceptibility disease involving antibody deficiency and aberrant TFH cells. *Science translational medicine* **11** (2019), doi:10.1126/scitranslmed.aau3776.

907 37. S. Crotty, T Follicular Helper Cell Differentiation, Function, and Roles in Disease.
908 *Immunity* **41**, 529–542 (2014).

909 38. E. Godefroy, H. Zhong, P. Pham, D. Friedman, K. Yazdanbakhsh, TIGIT-positive
910 circulating follicular helper T cells display robust B-cell help functions: potential role in
911 sickle cell alloimmunization. *Haematologica* **100**, 1415–1425 (2015).

912 39. N. M. Edner, L. P. Houghton, E. Ntavli, C. Rees-Spear, L. Petersone, C. Wang, A. Fabri,
913 Y. Elfaki, A. R. Gonzalez, R. Brown, K. Kisand, P. Peterson, L. E. McCoy, L. S. K. Walker,
914 TIGIT+Tfh show poor B-helper function and negatively correlate with SARS-CoV-2
915 antibody titre. *Front. Immunol.* **15**, 1395684 (2024).

916 40. A. Ianevski, A. K. Giri, T. Aittokallio, Fully-automated and ultra-fast cell-type
917 identification using specific marker combinations from single-cell transcriptomic data. *Nat.*
918 *Commun.* **13**, 1246 (2022).

919 41. N. P. Smith, B. Ruiter, Y. V. Virkud, A. A. Tu, B. Monian, J. J. Moon, J. C. Love, W. G.
920 Shreffler, Identification of antigen-specific TCR sequences based on biological and statistical
921 enrichment in unselected subjects. *JCI Insight* **6**, e140028 (2021).

922 42. V. Venturi, K. Kedzierska, D. A. Price, P. C. Doherty, D. C. Douek, S. J. Turner, M. P.
923 Davenport, Sharing of T cell receptors in antigen-specific responses is driven by convergent
924 recombination. *Proc. Natl. Acad. Sci.* **103**, 18691–18696 (2006).

925 43. M. Z. M. Zheng, L. Burmas, H.-X. Tan, M.-C. Trieu, H. J. Lee, D. Rawlinson, A. Haque,
926 S. J. Kent, A. K. Wheatley, J. A. Juno, Deconvoluting TCR-dependent & -independent
927 activation is vital for reliable Ag-specific CD4+ T cell characterization by AIM assay.
928 *bioRxiv* , 2024.12.10.627643 (2024).

929 44. I. Wahl, A. S. Obraztsova, J. Puchan, R. Hundsdorfer, S. Chakravarty, B. K. L. Sim, S. L.
930 Hoffman, P. G. Kremsner, B. Mordmüller, H. Wardemann, Clonal evolution and TCR
931 specificity of the human TFH cell response to Plasmodium falciparum CSP. *Sci Immunol* **7**,
932 eabm9644 (2022).

933 45. J. A. Juno, H.-X. Tan, W. S. Lee, A. Reynaldi, H. G. Kelly, K. Wragg, R. Esterbauer, H.
934 E. Kent, C. J. Batten, F. L. Mordant, N. A. Gherardin, P. Pymm, M. H. Dietrich, N. E. Scott,
935 W.-H. Tham, D. I. Godfrey, K. Subbarao, M. P. Davenport, S. J. Kent, A. K. Wheatley,
936 Humoral and circulating follicular helper T cell responses in recovered patients with COVID-
937 19. *Nature medicine* , 1–22 (2020).

938 46. M. T. Wong, J. Chen, S. Narayanan, W. Lin, R. Anicete, H. T. K. Kiaang, M. A. C. D.
939 Lafaille, M. Poidinger, E. W. Newell, Mapping the Diversity of Follicular Helper T Cells in
940 Human Blood and Tonsils Using High-Dimensional Mass Cytometry Analysis. *CellReports*
941 **11**, 1822–1833 (2015).

942 47. K. Lederer, E. Bettini, K. Parvathaneni, M. M. Painter, D. Agarwal, K. A. Lundgreen, M.
943 Weirick, K. Muralidharan, D. Castano, R. R. Goel, X. Xu, E. M. Drapeau, S. Gouma, J. T.
944 Ort, M. Awofolaju, A. R. Greenplate, C. L. Coz, N. Romberg, J. Trofe-Clark, G. Malat, L.
945 Jones, M. Rosen, D. Weiskopf, A. Sette, B. Besharatian, M. Kaminiski, S. E. Hensley, P.
946 Bates, E. J. Wherry, A. Naji, V. Bhoj, M. Locci, Germinal center responses to SARS-CoV-2

947 mRNA vaccines in healthy and immunocompromised individuals. *Cell* (2022),
948 doi:10.1016/j.cell.2022.01.027.

949 48. C. S. Nelson, P. T. Sage, TFH cell responses endure in human lymph nodes after
950 vaccination. *Nat. Immunol.* , 1–3 (2024).

951 49. P. A. Mudd, A. A. Minervina, M. V. Pogorelyy, J. S. Turner, W. Kim, E. Kalaidina, J.
952 Petersen, A. J. Schmitz, T. Lei, A. Haile, A. M. Kirk, R. C. Mettelman, J. C. Crawford, T. H.
953 O. Nguyen, L. C. Rowntree, E. Rosati, K. A. Richards, A. J. Sant, M. K. Klebert, T. Suessen,
954 W. D. Middleton, S. S. Team, J. H. Estepp, S. Schultz-Cherry, M. A. McGargill, A. Gaur, J.
955 Hoffman, M. Mori, L. Tang, E. Tuomanen, R. Webby, R. T. Hayden, H. Hakim, D. R.
956 Hijano, K. J. Allison, E. K. Allen, R. Bajracharya, W. Awad, L.-A. V. de Velde, B. L. Clark,
957 T. L. Wilson, A. Souquette, A. Castellaw, R. H. Dallas, A. Gowen, T. P. Fabrizio, C.-Y. Lin,
958 D. C. Brice, S. Cherry, E. K. Roubidoux, V. Cortez, P. Freiden, N. Wohlgemuth, K. Whitt, J.
959 Wolf, S. A. Teefey, J. A. O'Halloran, R. M. Presti, K. Kedzierska, J. Rossjohn, P. G.
960 Thomas, A. H. Ellebedy, SARS-CoV-2 mRNA vaccination elicits a robust and persistent T
961 follicular helper cell response in humans. *Cell* **185**, 603-613.e15 (2022).

962 50. S. Kho, L. Qotrunnada, L. Leonardo, B. Andries, P. A. I. Wardani, A. Fricot, B. Henry,
963 D. Hardy, N. I. Margyaningsih, D. Apriyanti, A. M. Puspitasari, P. Prayoga, L. Trianty, E.
964 Kenangalem, F. Chretien, I. Safeukui, H. A. del Portillo, C. Fernandez-Becerra, E. Meibalan,
965 M. Marti, R. N. Price, T. Woodberry, P. A. Ndour, B. M. Russell, T. W. Yeo, G. Minigo, R.
966 Noviyanti, J. R. Poespoprodjo, N. C. Siregar, P. A. Buffet, N. M. Anstey, Hidden Biomass of
967 Intact Malaria Parasites in the Human Spleen. *New Engl J Med* **384**, 2067–2069 (2021).

968 51. S. Kho, L. Qotrunnada, L. Leonardo, B. Andries, P. A. I. Wardani, A. Fricot, B. Henry,
969 D. Hardy, N. I. Margyaningsih, D. Apriyanti, A. M. Puspitasari, P. Prayoga, L. Trianty, E.
970 Kenangalem, F. Chretien, V. Brousse, I. Safeukui, H. A. del Portillo, C. Fernandez-Becerra,
971 E. Meibalan, M. Marti, R. N. Price, T. Woodberry, P. A. Ndour, B. M. Russell, T. W. Yeo,
972 G. Minigo, R. Noviyanti, J. R. Poespoprodjo, N. C. Siregar, P. A. Buffet, N. M. Anstey,
973 Evaluation of splenic accumulation and colocalization of immature reticulocytes and
974 Plasmodium vivax in asymptomatic malaria: A prospective human splenectomy study. *Plos*
975 *Med* **18**, e1003632 (2021).

976 52. J. S. McCarthy, S. Sekuloski, P. M. Griffin, S. Elliott, N. Douglas, C. Peatey, R. Rockett,
977 P. O'Rourke, L. Marquart, C. Hermsen, S. Duparc, J. Möhrle, K. R. Trenholme, A. J.
978 Humberstone, L. von Seidlein, Ed. A pilot randomised trial of induced blood-stage
979 Plasmodium falciparum infections in healthy volunteers for testing efficacy of new
980 antimalarial drugs. *PLoS ONE* **6**, e21914 (2011).

981 53. R. J. Rockett, S. J. Tozer, C. Peatey, S. Bialasiewicz, D. M. Whiley, M. D. Nissen, K.
982 Trenholme, J. S. M. Carthy, T. P. Sloots, A real-time, quantitative PCR method using
983 hydrolysis probes for the monitoring of Plasmodium falciparum load in experimentally
984 infected human volunteers. *Malaria Journal* **10**, 48 (2011).

985 54. A. H. Gaur, J. S. McCarthy, J. C. Panetta, R. H. Dallas, J. Woodford, L. Tang, A. M.
986 Smith, T. B. Stewart, K. C. Branum, B. B. Freeman, N. D. Patel, E. John, S. Chalon, S. Ost,
987 R. N. Heine, J. L. Richardson, R. Christensen, P. M. Flynn, Y. V. Gessel, B. Mitasev, J. J.
988 Möhrle, F. Gusovsky, L. Bebrevska, R. K. Guy, Safety, tolerability, pharmacokinetics, and
989 antimalarial efficacy of a novel Plasmodium falciparum ATP4 inhibitor SJ733: a first-in-

990 human and induced blood-stage malaria phase 1a/b trial. *Lancet Infect. Dis.* **20**, 964–975
991 (2020).

992 55. J. S. McCarthy, C. Donini, S. Chalon, J. Woodford, L. Marquart, K. A. Collins, F. D.
993 Rozenberg, D. A. Fidock, M. H. Cherkaoui-Rbati, N. Gobeau, J. J. Möhrle, A Phase 1,
994 Placebo-controlled, Randomized, Single Ascending Dose Study and a Volunteer Infection
995 Study to Characterize the Safety, Pharmacokinetics, and Antimalarial Activity of the
996 Plasmodium Phosphatidylinositol 4-Kinase Inhibitor MMV390048. *Clin. Infect. Dis.* **71**,
997 e657–e664 (2020).

998 56. K. A. Collins, C. Y. Wang, M. Adams, H. Mitchell, M. Rampton, S. Elliott, I. J. Reuling,
999 T. Bousema, R. Sauerwein, S. Chalon, J. J. Möhrle, J. S. McCarthy, A controlled human
1000 malaria infection model enabling evaluation of transmission-blocking interventions. *The*
1001 *Journal of clinical investigation* **128**, 1551–1562 (2018).

1002 57. T. M. Ashhurst, F. Marsh-Wakefield, G. H. Putri, A. G. Spiteri, D. Shinko, M. N. Read,
1003 A. L. Smith, N. J. C. King, Integration, exploration, and analysis of high-dimensional single-
1004 cell cytometry data using Spectre. *Cytom Part A* (2021), doi:10.1002/cyto.a.24350.

1005 58. X. Huang, Y. Huang, Cellsnp-lite: an efficient tool for genotyping single cells.
1006 *Bioinformatics* **37**, 4569–4571 (2021).

1007 59. T. 1000 G. P. Consortium, A. Auton, G. R. Abecasis, D. M. Altshuler, R. M. Durbin, G.
1008 R. Abecasis, D. R. Bentley, A. Chakravarti, A. G. Clark, P. Donnelly, E. E. Eichler, P. Flicek,
1009 S. B. Gabriel, R. A. Gibbs, E. D. Green, M. E. Hurles, B. M. Knoppers, J. O. Korbel, E. S.
1010 Lander, C. Lee, H. Lehrach, E. R. Mardis, G. T. Marth, G. A. McVean, D. A. Nickerson, J. P.
1011 Schmidt, S. T. Sherry, J. Wang, R. K. Wilson, R. A. Gibbs, E. Boerwinkle, H. Doddapaneni,
1012 Y. Han, V. Korchina, C. Kovar, S. Lee, D. Muzny, J. G. Reid, Y. Zhu, J. Wang, Y. Chang, Q.
1013 Feng, X. Fang, X. Guo, M. Jian, H. Jiang, X. Jin, T. Lan, G. Li, J. Li, Y. Li, S. Liu, X. Liu, Y.
1014 Lu, X. Ma, M. Tang, B. Wang, G. Wang, H. Wu, R. Wu, X. Xu, Y. Yin, D. Zhang, W.
1015 Zhang, J. Zhao, M. Zhao, X. Zheng, E. S. Lander, D. M. Altshuler, S. B. Gabriel, N. Gupta,
1016 N. Gharani, L. H. Toji, N. P. Gerry, A. M. Resch, P. Flicek, J. Barker, L. Clarke, L. Gil, S. E.
1017 Hunt, G. Kelman, E. Kulesha, R. Leinonen, W. M. McLaren, R. Radhakrishnan, A. Roa, D.
1018 Smirnov, R. E. Smith, I. Streeter, A. Thormann, I. Toneva, B. Vaughan, X. Zheng-Bradley,
1019 D. R. Bentley, R. Grocock, S. Humphray, T. James, Z. Kingsbury, H. Lehrach, R. Sudbrak,
1020 M. W. Albrecht, V. S. Amstislavskiy, T. A. Borodina, M. Lienhard, F. Mertes, M. Sultan, B.
1021 Timmermann, M.-L. Yaspo, E. R. Mardis, R. K. Wilson, L. Fulton, R. Fulton, S. T. Sherry,
1022 V. Ananiev, Z. Belaia, D. Beloslyudtsev, N. Bouk, C. Chen, D. Church, R. Cohen, C. Cook,
1023 J. Garner, T. Hefferon, M. Kimelman, C. Liu, J. Lopez, P. Meric, C. O'Sullivan, Y.
1024 Ostapchuk, L. Phan, S. Ponomarov, V. Schneider, E. Shekhtman, K. Sirotkin, D. Slotta, H.
1025 Zhang, G. A. McVean, R. M. Durbin, S. Balasubramaniam, J. Burton, P. Danecek, T. M.
1026 Keane, A. Kolb-Kokocinski, S. McCarthy, J. Stalker, M. Quail, J. P. Schmidt, C. J. Davies, J.
1027 Gollub, T. Webster, B. Wong, Y. Zhan, A. Auton, C. L. Campbell, Y. Kong, A. Marcketta,
1028 R. A. Gibbs, F. Yu, L. Antunes, M. Bainbridge, D. Muzny, A. Sabo, Z. Huang, J. Wang, L. J.
1029 M. Coin, L. Fang, X. Guo, X. Jin, G. Li, Q. Li, Y. Li, Z. Li, H. Lin, B. Liu, R. Luo, H. Shao,
1030 Y. Xie, C. Ye, C. Yu, F. Zhang, H. Zheng, H. Zhu, C. Alkan, E. Dal, F. Kahveci, G. T.
1031 Marth, E. P. Garrison, D. Kural, W.-P. Lee, W. F. Leong, M. Stromberg, A. N. Ward, J. Wu,
1032 M. Zhang, M. J. Daly, M. A. DePristo, R. E. Handsaker, D. M. Altshuler, E. Banks, G.
1033 Bhatia, G. del Angel, S. B. Gabriel, G. Genovese, N. Gupta, H. Li, S. Kashin, E. S. Lander, S.
1034 A. McCarroll, J. C. Nemesh, R. E. Poplin, S. C. Yoon, J. Lihm, V. Makarov, A. G. Clark, S.

Gottipati, A. Keinan, J. L. Rodriguez-Flores, J. O. Korbel, T. Rausch, M. H. Fritz, A. M. Stütz, P. Flicek, K. Beal, L. Clarke, A. Datta, J. Herrero, W. M. McLaren, G. R. S. Ritchie, R. E. Smith, D. Zerbino, X. Zheng-Bradley, P. C. Sabeti, I. Shlyakhter, S. F. Schaffner, J. Vitti, D. N. Cooper, E. V. Ball, P. D. Stenson, D. R. Bentley, B. Barnes, M. Bauer, R. K. Cheetham, A. Cox, M. Eberle, S. Humphray, S. Kahn, L. Murray, J. Peden, R. Shaw, E. E. Kenny, M. A. Batzer, M. K. Konkel, J. A. Walker, D. G. MacArthur, M. Lek, R. Sudbrak, V. S. Amstislavskiy, R. Herwig, E. R. Mardis, L. Ding, D. C. Koboldt, D. Larson, K. Ye, S. Gravel, A. Swaroop, E. Chew, T. Lappalainen, Y. Erlich, M. Gymrek, T. F. Willems, J. T. Simpson, M. D. Shriver, J. A. Rosenfeld, C. D. Bustamante, S. B. Montgomery, F. M. D. L. Vega, J. K. Byrnes, A. W. Carroll, M. K. DeGorter, P. Lacroute, B. K. Maples, A. R. Martin, A. Moreno-Estrada, S. S. Shringarpure, F. Zakharia, E. Halperin, Y. Baran, C. Lee, E. Cerveira, J. Hwang, A. Malhotra, D. Plewczynski, K. Radew, M. Romanovitch, C. Zhang, F. C. L. Hyland, D. W. Craig, A. Christoforides, N. Homer, T. Izatt, A. A. Kurdoglu, S. A. Sinari, K. Squire, S. T. Sherry, C. Xiao, J. Sebat, D. Antaki, M. Gujral, A. Noor, K. Ye, E. G. Burchard, R. D. Hernandez, C. R. Gignoux, D. Haussler, S. J. Katzman, W. J. Kent, B. Howie, A. Ruiz-Linares, E. T. Dermitzakis, S. E. Devine, G. R. Abecasis, H. M. Kang, J. M. Kidd, T. Blackwell, S. Caron, W. Chen, S. Emery, L. Fritsche, C. Fuchsberger, G. Jun, B. Li, R. Lyons, C. Scheller, C. Sidore, S. Song, E. Sliwerska, D. Taliun, A. Tan, R. Welch, M. K. Wing, X. Zhan, P. Awadalla, A. Hodgkinson, Y. Li, X. Shi, A. Quitadamo, G. Lunter, G. A. McVean, J. L. Marchini, S. Myers, C. Churchhouse, O. Delaneau, A. Gupta-Hinch, W. Kretzschmar, Z. Iqbal, I. Mathieson, A. Menelaou, A. Rimmer, D. K. Xifara, T. K. Oleksyk, Y. Fu, X. Liu, M. Xiong, L. Jorde, D. Witherspoon, J. Xing, E. E. Eichler, B. L. Browning, S. R. Browning, F. Hormozdiari, P. H. Sudmant, E. Khurana, R. M. Durbin, M. E. Hurles, C. Tyler-Smith, C. A. Albers, Q. Ayub, S. Balasubramaniam, Y. Chen, V. Colonna, P. Danecek, L. Jostins, T. M. Keane, S. McCarthy, K. Walter, Y. Xue, M. B. Gerstein, A. Abyzov, S. Balasubramanian, J. Chen, D. Clarke, Y. Fu, A. O. Harmanci, M. Jin, D. Lee, J. Liu, X. J. Mu, J. Zhang, Y. Zhang, Y. Li, R. Luo, H. Zhu, C. Alkan, E. Dal, F. Kahveci, G. T. Marth, E. P. Garrison, D. Kural, W.-P. Lee, A. N. Ward, J. Wu, M. Zhang, S. A. McCarroll, R. E. Handsaker, D. M. Altshuler, E. Banks, G. del Angel, G. Genovese, C. Hartl, H. Li, S. Kashin, J. C. Nemesh, K. Shakir, S. C. Yoon, J. Lihm, V. Makarov, J. Degenhardt, J. O. Korbel, M. H. Fritz, S. Meiers, B. Raeder, T. Rausch, A. M. Stütz, P. Flicek, F. P. Casale, L. Clarke, R. E. Smith, O. Stegle, X. Zheng-Bradley, D. R. Bentley, B. Barnes, R. K. Cheetham, M. Eberle, S. Humphray, S. Kahn, L. Murray, R. Shaw, E.-W. Lameijer, M. A. Batzer, M. K. Konkel, J. A. Walker, L. Ding, I. Hall, K. Ye, P. Lacroute, C. Lee, E. Cerveira, A. Malhotra, J. Hwang, D. Plewczynski, K. Radew, M. Romanovitch, C. Zhang, D. W. Craig, N. Homer, D. Church, C. Xiao, J. Sebat, D. Antaki, V. Bafna, J. Michaelson, K. Ye, S. E. Devine, E. J. Gardner, G. R. Abecasis, J. M. Kidd, R. E. Mills, G. Dayama, S. Emery, G. Jun, X. Shi, A. Quitadamo, G. Lunter, G. A. McVean, K. Chen, X. Fan, Z. Chong, T. Chen, D. Witherspoon, J. Xing, E. E. Eichler, M. J. Chaisson, F. Hormozdiari, J. Huddleston, M. Malig, B. J. Nelson, P. H. Sudmant, N. F. Parrish, E. Khurana, M. E. Hurles, B. Blackburne, S. J. Lindsay, Z. Ning, K. Walter, Y. Zhang, M. B. Gerstein, A. Abyzov, J. Chen, D. Clarke, H. Lam, X. J. Mu, C. Sisu, J. Zhang, Y. Zhang, R. A. Gibbs, F. Yu, M. Bainbridge, D. Challis, U. S. Evani, C. Kovar, J. Lu, D. Muzny, U. Nagaswamy, J. G. Reid, A. Sabo, J. Yu, X. Guo, W. Li, Y. Li, R. Wu, G. T. Marth, E. P. Garrison, W. F. Leong, A. N. Ward, G. del Angel, M. A. DePristo, S. B. Gabriel, N. Gupta, C. Hartl, R. E. Poplin, A. G. Clark, J. L. Rodriguez-Flores, P. Flicek, L. Clarke, R. E. Smith, X. Zheng-Bradley, D. G. MacArthur, E. R. Mardis, R. Fulton, D. C. Koboldt, S. Gravel, C. D. Bustamante, D. W. Craig, A. Christoforides, N. Homer, T. Izatt, S. T. Sherry, C. Xiao, E. T. Dermitzakis, G. R. Abecasis, H. M. Kang, G. A. McVean, M. B. Gerstein, S. Balasubramanian, L. Habegger, H. Yu, P. Flicek, L. Clarke, F. Cunningham, I. Dunham, D. Zerbino, X. Zheng-Bradley, K. Lage, J. B. Jespersen, H. Horn, S. B.

1085 Montgomery, M. K. DeGorter, E. Khurana, C. Tyler-Smith, Y. Chen, V. Colonna, Y. Xue,
1086 M. B. Gerstein, S. Balasubramanian, Y. Fu, D. Kim, A. Auton, A. Marcketta, R. Desalle, A.
1087 Narechania, M. A. W. Sayres, E. P. Garrison, R. E. Handsaker, S. Kashin, S. A. McCarroll, J.
1088 L. Rodriguez-Flores, P. Flicek, L. Clarke, X. Zheng-Bradley, Y. Erlich, M. Gymrek, T. F.
1089 Willems, C. D. Bustamante, F. L. Mendez, G. D. Poznik, P. A. Underhill, C. Lee, E.
1090 Cerveira, A. Malhotra, M. Romanovitch, C. Zhang, G. R. Abecasis, L. Coin, H. Shao, D.
1091 Mittelman, C. Tyler-Smith, Q. Ayub, R. Banerjee, M. Cerezo, Y. Chen, T. W. Fitzgerald, S.
1092 Louzada, A. Massaia, S. McCarthy, G. R. Ritchie, Y. Xue, F. Yang, R. A. Gibbs, C. Kovar,
1093 D. Kalra, W. Hale, D. Muzny, J. G. Reid, J. Wang, X. Dan, X. Guo, G. Li, Y. Li, C. Ye, X.
1094 Zheng, D. M. Altshuler, P. Flicek, L. Clarke, X. Zheng-Bradley, D. R. Bentley, A. Cox, S.
1095 Humphray, S. Kahn, R. Sudbrak, M. W. Albrecht, M. Lienhard, D. Larson, D. W. Craig, T.
1096 Izatt, A. A. Kurdoglu, S. T. Sherry, C. Xiao, D. Haussler, G. R. Abecasis, G. A. McVean, R.
1097 M. Durbin, S. Balasubramaniam, T. M. Keane, S. McCarthy, J. Stalker, A. Chakravarti, B.
1098 M. Knoppers, G. R. Abecasis, K. C. Barnes, C. Beiswanger, E. G. Burchard, C. D.
1099 Bustamante, H. Cai, H. Cao, R. M. Durbin, N. P. Gerry, N. Gharani, R. A. Gibbs, C. R.
1100 Gignoux, S. Gravel, B. Henn, D. Jones, L. Jorde, J. S. Kaye, A. Keinan, A. Kent, A.
1101 Kerasidou, Y. Li, R. Mathias, G. A. McVean, A. Moreno-Estrada, P. N. Ossorio, M. Parker,
1102 A. M. Resch, C. N. Rotimi, C. D. Royal, K. Sandoval, Y. Su, R. Sudbrak, Z. Tian, S.
1103 Tishkoff, L. H. Toji, C. Tyler-Smith, M. Via, Y. Wang, H. Yang, L. Yang, J. Zhu, W.
1104 Bodmer, G. Bedoya, A. Ruiz-Linares, Z. Cai, Y. Gao, J. Chu, L. Peltonen, A. Garcia-
1105 Montero, A. Orfao, J. Dutil, J. C. Martinez-Cruzado, T. K. Oleksyk, K. C. Barnes, R. A.
1106 Mathias, A. Hennis, H. Watson, C. McKenzie, F. Qadri, R. LaRocque, P. C. Sabeti, J. Zhu,
1107 X. Deng, P. C. Sabeti, D. Asogun, O. Folarin, C. Happi, O. Omoniwa, M. Stremlau, R.
1108 Tariyal, M. Jallow, F. S. Joof, T. Corrah, K. Rockett, D. Kwiatkowski, J. Kooner, T. T.
1109 Hiê`n, S. J. Dunstan, N. T. Hang, R. Fonnie, R. Garry, L. Kanneh, L. Moses, P. C. Sabeti, J.
1110 Schieffelin, D. S. Grant, C. Gallo, G. Poletti, D. Saleheen, A. Rasheed, L. D. Brooks, A. L.
1111 Felsenfeld, J. E. McEwen, Y. Vaydylevich, E. D. Green, A. Duncanson, M. Dunn, J. A.
1112 Schloss, J. Wang, H. Yang, A. Auton, L. D. Brooks, R. M. Durbin, E. P. Garrison, H. M.
1113 Kang, J. O. Korbel, J. L. Marchini, S. McCarthy, G. A. McVean, G. R. Abecasis, A global
1114 reference for human genetic variation. *Nature* **526**, 68–74 (2015).

1115 60. Y. Huang, D. J. McCarthy, O. Stegle, Vireo: Bayesian demultiplexing of pooled single-
1116 cell RNA-seq data without genotype reference. *Genome Biol.* **20**, 273 (2019).

1117 61. Y. Hao, T. Stuart, M. H. Kowalski, S. Choudhary, P. Hoffman, A. Hartman, A.
1118 Srivastava, G. Molla, S. Madad, C. Fernandez-Granda, R. Satija, Dictionary learning for
1119 integrative, multimodal and scalable single-cell analysis. *Nat. Biotechnol.* **42**, 293–304
1120 (2024).

1121 62. S. Marsh, M. Salmon, P. Hoffma, kew24, *samuel-marsh/scCustomize Version 3.0.1*
1122 (Zenodo, 2024; https://zenodo.org/records/14529706).

1123 63. S. Choudhary, R. Satija, Comparison and evaluation of statistical error models for
1124 scRNA-seq. *Genome Biol.* **23**, 27 (2022).

1125 64. M. D. Robinson, G. K. Smyth, Small-sample estimation of negative binomial dispersion,
1126 with applications to SAGE data. *Biostatistics* **9**, 321–332 (2008).

1127